THE UNIVERSITY of EDINBURGH

Edinburgh Research Explorer

Inflammation-induced formation of fat-associated lymphoid clusters

Citation for published version:
Benezech, C, Luu, N-T, Walker, J, Kruglov, A, Loo, Y, Nakamura, K, Zhang, Y, Jones, L, Nayar, S, Flores-Langarica, A, McIntosh, A, Marshall, J, Barone, F, Besra, G, Miles, K, Allen, J, Gray, M, Kollias, G, Cunningham, AF, Withers, DR, Toellner, K, Jones, N, Veldhoen, M, Nedospasov, S, McKenzie, A & Caamano, J 2015, 'Inflammation-induced formation of fat-associated lymphoid clusters' Nature Immunology. DOI: 10.1038/ni.3215

Digital Object Identifier (DOI):
10.1038/ni.3215

Link:
Link to publication record in Edinburgh Research Explorer

Document Version:
Peer reviewed version

Published In:
Nature Immunology

Publisher Rights Statement:
This is the final accepted manuscript.

General rights
Copyright for the publications made accessible via the Edinburgh Research Explorer is retained by the author(s) and / or other copyright owners and it is a condition of accessing these publications that users recognise and abide by the legal requirements associated with these rights.

Take down policy
The University of Edinburgh has made every reasonable effort to ensure that Edinburgh Research Explorer content complies with UK legislation. If you believe that the public display of this file breaches copyright please contact openaccess@ed.ac.uk providing details, and we will remove access to the work immediately and investigate your claim.

OPEN ACCESS

Download date: 05. Apr. 2019

Inflammation-induced formation of Fat Associated Lymphoid Clusters requires TNFR signaling and Natural Killer T cells

Cécile Bénézech[1*#], Nguyet-Thin Luu[1§], Jennifer A. Walker[2§], Andrei A. Kruglov[3, 4], Yunhua Loo[5], Kyoko Nakamura[1], Yang Zhang[1], Saba Nayar[1], Lucy H. Jones[6], Adriana Flores-Langarica[1], Alistair McIntosh[1], Jennifer Marshall[1], Francesca Barone[1], Gurdyal Besra[7], Katherine Miles[8], Judith E. Allen[6], Mohini Gray[8], George Kollias[9], Adam F. Cunningham[1], David R. Withers[1], Kai Michael Toellner[1], Nick D. Jones[1], Marc Veldhoen[5], Sergei A. Nedospasov[3, 4], Andrew N.J. McKenzie[2], and Jorge H. Caamaño[1*]

[1]School of Immunity and Infection, IBR-MRC Centre for Immune Regulation, College of Medical and Dental Sciences, University of Birmingham, Birmingham, B15 2TT, UK, [2]MRC Laboratory of Molecular Biology, Cambridge, UK, [3]German Rheumatism Research Center, Berlin, Germany, [4]Engelhardt Institute of Molecular Biology and Lomonosov Moscow State University, Moscow, Russia, [5]The Babraham Institute, Cambridge, UK, [6]Institute of Immunology and Infection Research, University of Edinburgh, Edinburgh, [7]College of Life and Environmental Sciences, University of Birmingham, UK, [8]Centre for Cardiovascular Sciences, Edinburgh, UK, [9]Fleming Institute, Athens, Greece.

*Correspondence: c.benezech@staffmail.ed.ac.uk (CB), j.caamano@bham.ac.uk (JC).

[#]Present Address: BHF/UoE Centre for Cardiovascular Sciences, University of Edinburgh, Edinburgh, UK

[§] These authors contributed equally to this work

Running Title: iNKT cells and TNFα are required for FALC formation

Abstract: 120 words

ABSTRACT

Fat Associated Lymphoid Clusters (FALCs) are a recently discovered type of lymphoid tissue associated with visceral fat. Here we show that the distribution of FALCs is heterogeneous with the pericardium containing a very large number. FALCs contribute to the retention of B1 cells in the peritoneal cavity through high expression of CXCL13 and support B cell proliferation and germinal centre differentiation during peritoneal immune challenges. Their formation is induced by inflammation, which triggers an important recruitment of myeloid cells that express TNF necessary for TNFR-signaling in stromal cells. Finally, we demonstrate that NKT cells play a crucial role in the inducible formation of FALCs, placing these clusters at the centre of innate like B and T cell activation during serosal immune responses.

INTRODUCTION

The peritoneal and pleural cavities constitute compartments with special characteristics to support rapid immune responses when the integrity of the intestine and the lungs is compromised/lost. A common feature of these compartments is the presence of a significant fraction of B1 cells that encompass diverse mouse innate-like B cell populations producing natural antibodies vital for the early control of infections, protecting against auto-immunity and contributing to adaptive immunity[1–7]. These B1 cells recirculate between the peritoneal space and the omentum[8], a sheet of intra-abdominal adipose tissue containing lymphoid structures called “milky spots”, that acts as a direct filter of the peritoneal cavity[9–12]. Upon peritoneal inflammation the number and size of milky spots increases and the recruitment of lymphocytes and macrophages phagocytosing particles and pathogens is dramaticaly augmented[9, 11, 12]. The omentum also acts as a secondary lymphoid structure that promotes immunity to peritoneal antigens[10, 12].

More recently, the existence of B cell rich clusters in adipose tissue has been extended to the rest of the visceral adipose tissue (VAT) in the peritoneal and pleural cavity[13, 14]. Moro and collaborators named them Fat Associated Lymphoid Clusters (FALCs)[14]. Their development was associated with the presence of Group 2 innate lymphoid cells (ILC2, also known as Innate type 2 helper cells/Nuocytes/Natural helper cells[14–17]) in VAT, yet no direct evidence has shown that ILC2s induce formation of FALCs[14]. The exact composition of these clusters, their relative distribution in the different VAT deposits as well as their function and the mechanisms regulating their formation remain unknown.

Here we show that the distribution of lymphoid structures in adipose tissue is very heterogeneous, with the omentum, the pericardium and mediastinum being the tissues containing the largest number of FALCs. We report that the development of FALCs is regulated by unique cellular and molecular mechanisms that in contrast to other secondary lymphoid tissues do not involve lymphoid tissue inducer (LTi) cells/ILC3 and the Lymphotoxin Beta Receptor (LTβR) pathway[18–20]. Their postnatal formation was partly dependent on TNFR signalling and the presence of the commensal flora. The stromal cells of FALCs expressed high levels of CXCL13 crucial for the recruitment and retention of B1 and B2 cells in the peritoneum. Inflammation-induced formation of FALCs required TNF expression by myeloid cells and TNFR-signalling in stromal cells. Peritoneal immunization with T-independent and T-dependent antigens induced B cell differentiation into plasma cells and germinal centre (GC)-like B cells in FALCs indicating an important function of

these clusters during immune responses. Finally, we show that invariant Natural Killer T (iNKT) cells, a subset of T cells enriched in adipose tissues, and IL-13 played a key role in inflammation-induced FALC formation.

RESULTS

Visualisation and characterisation of FALCs

The anatomical distribution of FALCs in adipose tissue renders impractical the methods generally used for the visualisation and isolation of lymphoid structures (cryo-sections and paraffin embedded sections). We therefore performed whole-mount immunofluorescence staining of the main VAT found in the peritoneal and pleural cavities, which allowed, with a fluorescence stereomicroscope, the visualisation (Fig. 1a) and enumeration of the $CD45^+$ cell clusters present in the omental, gonadal, mesenteric, mediastinal and pericardial adipose tissue. In the peritoneal cavity, the omentum was the fat depot with the highest density of lymphoid clusters (8000 clusters/g) with a mean of 80 milky spots per omentum. The density of FALCs was highest in the mesenteric fat depot (120 clusters/g with a mean of 16 clusters per mesentery) but was very low in the gonadal adipose tissue (8 clusters/g) with a mean of 1-2 clusters per depot (Fig.1b-c). In the pleural cavity, the fat depot with the highest density of lymphoid clusters was the pericardium (5400 clusters/g) with a mean of 40 clusters per pericardium. The mediastinum with a density of 2100 clusters/g and a mean of 9 clusters per mediastinum, accounts for the rest of the FALCs in the pleural cavity (Fig.1b-c). This analysis revealed the high heterogeneity in the lymphoid cluster content of adipose tissues, ranging from complete absence or very low numbers in the case of the subcutaneous adipose tissue and gonadal adipose tissue, respectively, to a very high density in the case of the omentum, the pericardium and mediastinum. The omentum and the pericardium contained approximately eighty per cent of the lymphoid clusters in the peritoneum and pleural cavities respectively, while the rest of the clusters are present in the gonadal adipose tissue and the mediastinum (Fig 1c).

The cellular composition of the clusters was determined using a combination of stains with fluorescent Abs followed by isolation with a stereomicroscope and further confocal microscopy analysis. In resting conditions the clusters were mostly composed of IgM^+ B cells, with few $CD4^+$ T cells and very low numbers of $CD11b^+$ myeloid cells (Fig. 1d and Sup. Fig.1). Clusters of different sizes and degrees of B-T cell segregation could be observed in individual mice and in different fat depots with the largest clusters presenting a core of T cells surrounded by B cells (Sup. Fig.1). The high level of IgM expression on a fraction of B cells combined with the expression of CD11b on some of these IgM^{bright} B cells indicated the presence of B1 cells. We did not detect any differences in the

hematopoietic composition of FALCs from the mesenteries, mediastinum or pericardium that resembled the milky spots of the omentum (not shown). FALCs appeared to be highly vascularised, as shown by the presence of $CD31^+$ blood vessels. However, no clear connection with Lyve-1^+ lymphatic vasculature could be detected. Only scattered Lyve-1^+ macrophages were seen in close proximity of FALCs (Fig. 1e).

The mesenteric adipose tissues, where FALCs were easier to identify and enumerate, were used in the rest of the study to analyse the development and function of these structures. FALC formation was initiated after birth, with the first clusters identified in the mesenteries of two- to three-week old animals and their number increasing to reach a plateau at around 18 weeks of age (Fig 1f).

CXCL13 is highly expressed by stromal cells in FALCs

To understand how B and T cells were recruited to the FALCs, we assessed the expression of the homeostatic chemokines *Cxcl13*, *Ccl21* and *Ccl19* as well as the cytokine *Il-7* by qPCR analysis in isolated clusters as described in materials and methods. Cxcl13 expression was found to be particularly high in FALCs compared to the associated adipose tissue (>100 fold) or lymph nodes (LN) (10 fold). In contrast, *Ccl21*, *Ccl19* and *Il-7* transcripts were not enriched in FALCs compared to the other tissues analyzed (Fig. 2a). In agreement with these results, the number and composition of FALCs in CCL21- and CCL19-deficient mice (*Plt/plt)* and *Ccr7*$^{-/-}$ mice presented no differences with their WT counterparts (Fig. 2b-c). *Tnf* and *Ltβ* transcripts were both highly expressed in FALCs, which might reflect the high content of B cells in these clusters.

We further characterised the expression of CXCL13 in FALCs by immuno-fluorescence staining. We observed $CD45^-CXCL13^+$ stromal cells with an elongated morphology were present in the clusters (Fig. 2d) and resembled Follicular Dendritic Cells (FDCs). This prompted us to test whether LTβR and/or TNFR signalling were involved in inducing the expression of this chemokine, as is the case for spleen and LN FDCs[21–23]. However, we observed that $CXCL13^+$ cells were present in FALCs of *Ltβr*$^{-/-}$ and *Tnfr*1/2$^{-/-}$ mice, demonstrating that the expression of this chemokine by FALC stromal cells is independent of signals induced by these receptors (Fig. 2d). $CXCL13^+$ cells were also found in FALCs of *Rag2*$^{-/-}$ mice, indicating that signals delivered by B and T cells were not involved in the induction/maintenance of CXCL13 expression in these structures[24, 25].

To test whether CXCL13 expression is the basis of the recruitment of B cells in FALCs, we analysed cluster formation in the *Cxcr5*$^{-/-}$ mice, which are deficient for the

CXCL13 receptor. We found a normal number of FALCs forming in the mesenteries of these mice, but as expected a marked reduction in the B cells present in the clusters. This indicated that CXCL13 was not important for FALC formation but was essential for the recruitment of B cells (Fig. 2c-d). The mesenteries together with the omentum were previously identified as an important source of CXCL13 for the retention of B cells in the peritoneal cavity. Overall, we demonstrate that the presence of CXCL13 in the mesenteries is due to its specific expression by FALC stromal cells and not the surrounding adipose tissue.

FALCs support B cell proliferation and differentiation during peritoneal immune challenges

B1 cells are important for immune responses against T-independent (TI) antigens[2, 5, 26–31]. Therefore, to assess B cell responses in FALCs, we used the TI antigen 4-hydroxy-3-nitrophenylacetyl (NP)-Ficoll to immunise QM/QM ($IgH^{NP/NP}$ $Ig\kappa^{-/-}$) mice, which have a quasi-monoclonal primary B cell repertoire specific for NP[32]. We compared the proliferative response of B cells in FALCs, the peritoneal cavity, and the spleen in response to NP-Ficoll by determining the percentages of $Ki67^+$ B cells, 24 hours post intra-peritoneal (IP) immunisation, in enzymatically digested mesenteries (mesenteric LNs carefully removed), the peritoneal cavity lavage and the spleen. We found that both B1 and B2 cells rapidly started to proliferate in the mesenteries. Interestingly, the percentages of $Ki67^+$ proliferating B1 cells in the mesenteries was three times higher than the level of proliferation found in the peritoneal cavity lavage or the spleen, reaching 70% for B1a, 50% for B1b and 40% for B1c cells. Up to 40% of B2 cells also proliferated in response to NP-Ficoll (Supp. Fig. 2a-b). Whole mount staining of the mesenteries 24 hours after immunisation showed that the majority of B cells were located in FALCs and not dispersed in the adipose tissue. Moreover, FALCs showed a marked enlargement in their size and an increased level of IgM staining (Supp. Fig. 2c). Collectively, results from flow-cytometric and confocal analysis indicated that B cells were actively proliferating in FALCs. To confirm that FALC B cells were actively secreting IgM, we assessed the number of antibody-forming cells (AFC) four days after NP-Ficoll IP immunisation. To do this QMxB6 ($IgH^{NP/wt}$ $Ig\kappa^{-/wt}$) mice[33] were used, which contain 5% of NP-specific B cells. ELISpot analysis of cells isolated from the immunised animals confirmed an expansion of NP-specific B cells expressing IgM (Fig. 3a top). We also found a significant increase in cells that have undergone switching to IgG in FALCs and spleen (Fig. 3a bottom and Fig. 3b).

Further evidence of B cells undergoing Ig switching in FALCs was obtained by NP-Ficoll immunisation of Cγ1-CrexQMmTmG mice ($IgH^{NP/C_\gamma1Cre}$ $Ig\kappa^{-/-}$, $mTmG^{+/wt}$). These mice carry one copy of the Cre recombinase in the IgG1 heavy chain gene, induced during activation of Ig class switching[34], in combination with one copy of the NP-specific heavy chain from QM mice and the mTmG reporter[35]. This showed clusters of B blasts or plasmablasts that had undergone induction of Ig class switch recombination (Green) further supporting the ELISpot results (Fig. 3b). The early and preferential proliferation of B1 cells in FALCs, and the presence of IgM and IgG producing cells demonstrated that these clusters contribute to peritoneal cavity B1 cells immune responses to type II antigens.

The role of FALCs in T-dependent immune responses was tested by intra-venous (IV) adoptive transfer of peritoneal lavage cells from QM/QM ($IgH^{NP/NP}$ $Ig\kappa^{-/-}$)$EYFP^{+/-}$ mice into C57BL/6J recipients that were subsequently IP immunised with Alum precipitated-NP-OVA (Fig 3c). Flow cytometric analysis of cells isolated eight days after immunization showed a statistically significant increase in the frequency and number of Ag-specific B cells and $CD38^{-}GL7^{+}$ GC-like B cells in FALCs, spleen and mesenteric (m)LNs (Fig 3d-e and data not shown). An endogenous immune response was elicited by IP immunising C57BL/6J mice with Alum precipitated-Phycoerythrin (PE). In agreement with the results above, flow-cytometric analysis of FALCs, spleen and mLN showed a 20x increase in the proportion and number of PE-specific B cells and GC-like B cells (Fig 3f-h and data not shown). Taken together, these results indicate that FALCs act as true lymphoid tissues by supporting early activation of B cells during inflammation and differentiation towards plasma cells and germinal centre cells during adaptive immune responses in the peritoneal cavity.

FALC development is regulated by unique cellular and molecular mechanisms that are independent of LTi cells and the LTβR pathway.

The development of LNs and Peyer's patches is dependent on the activity of LTi cells and engagement of the LTβR[18–20]. To determine whether the formation of FALCs followed the same cellular and molecular cues, we assessed the presence of these clusters in the *Ltβr*$^{-/-}$, *Ltα*$^{-/-}$ and *Rorc*$^{-/-}$ mouse strains in which LN development is fully impaired[36–38]. We found no differences in the number and composition of FALCs in these strains compared to WT mice, indicating that the development of these clusters was independent of both LTi/ILC3 cells and LTβR engagement (Fig. 4a-b). To determine whether any other lymphoid cell type was involved in FALC formation, we analyzed the presence of these structures in

Rag2$^{-/-}$ mice, lacking lymphocytes, and the *Rag2*$^{-/-}\gamma c^{-/-}$ mice that are deficient in lymphocytes and ILCs. We found that while FALCs were present in normal numbers in *Rag2*$^{-/-}$ mice; they were absent in *Rag2*$^{-/-}\gamma c^{-/-}$ mice revealing a potential requirement for ILCs and/or NK cells to initiate cluster formation. *Il15*$^{-/-}$ mice have similar FALC numbers to their WT counterparts, ruling out a role for NK cells in the formation of these clusters (data not shown). Flow cytometric analysis of VAT in WT and *Rag2*$^{-/-}$ mice demonstrated the presence of Lin^{-}c-Kit^{+}Sca-1^{+}IL-7Rα^{+} ILCs type 2 (Supp. Fig 3a). In addition, more than 80% of the Lin^{-}CD90^{+}Sca-1^{+}NK1.1^{-} cells present in FALCs of *Rag2*$^{-/-}$ mice correspond to ILC2 cells further confirming the presence of these cells in the clusters[14] (Supp. Fig 3b). Moreover, immunofluorescence staining of mesenteries of *Rag2*$^{-/-}$ mice identified clusters of CD90^{+}CD11b^{-} cells in FALCs, that in the absence of T cells are likely to correspond to ILCs (Supp. Fig 3c).

As the LTα-LTβR pathway was not required for the formation of FALCs, we examined the role of TNF, another key regulator of lymphoid tissue organization[22, 23, 39]. In the double knockout mouse model for its receptors TNFR1 and TNFR2 (*Tnfr1/2*$^{-/-}$), we observed a two-fold reduction in the number of FALCs as well as a general decrease in the size of the clusters (Fig. 4a-b). Conversely, in the *Tnf*$^{+/\Delta ARE}$ mice, which carry a deletion that results in the accumulation of *Tnf* mRNA and protein, and the development of inflammatory diseases[40], we observed an eight-fold increase in FALC number and in the size of the clusters with respect to those present in WT littermates (Fig. 4a-b). Thus, we conclude that TNF signalling promoted the formation of FALCs.

Colonisation by the commensal flora is involved in the postnatal development and maturation of the Gut Associated Lymphoid Tissues (GALT)[41-44]. The postnatal development of FALCs suggested a similar mechanism. Indeed, Germ Free (GF) mice showed a two-fold reduction in the number of FALCs indicating that the commensal flora partly contributed to their formation (Fig. 4a-b). Overall, these analyses revealed that the formation of FALCs is entirely dependent on an innate lymphoid cell type different from LTi cells and other RORγt^{+} ILC3 cells and partly dependent on TNF signalling and colonisation by the commensal flora.

Peritoneal inflammation led to rapid formation of FALCs

Since the formation of FALCs was increased in *Tnf*$^{+/\Delta ARE}$ mice, we tested the effect of acute sterile peritonitis on FALC formation. Peritoneal inflammation driven by Zymosan led to a marked increase in the size and number of FALCs at day 3, with the clusters

becoming visible without counterstaining under the dissecting microscope (Fig. 4c) and their numbers doubling (Fig. 4d). The increase in size and number of the clusters was associated with a pronounced alteration in their composition. We found that inflammation induced a significant recruitment of $CD11b^+$ myeloid cells (Fig. 4e). Further immuno-fluorescence staining showed that the myeloid cells whithin FALCs were mostly $Gr1^{low/-}$ $Ly6C^{low/-}F4/80^+$ macrophages (Supp. Fig. 4). These observations indicate that FALC formation is inducible and that peritoneal inflammation leads to a general expansion and formation of the lymphoid clusters associated with VAT.

TNF expression by myeloid cells and TNFR1/2 signalling on stromal cells are necessary for FALC formation upon inflammation

Experiments with Zymosan revealed that formation of FALCs could be induced in adult mice by inflammation. The pro-inflammatory cytokine TNF, which promoted the formation of FALCs in non-immunised mice (Fig. 4a-b), was a strong candidate to be involved in the induction of these clusters upon inflammation. Immunisation with Zymosan in the *Tnfr1/2*$^{-/-}$ mice failed to induce de novo formation of clusters at day 3 post-injection as in WT mice, even though existing FALCs increased in size and recruited $CD11b^+$ myeloid cells (Fig. 5a).

We then asked whether TNF-R-signalling was required on stromal cells to induce formation of FALCs following Zymosan injection. To address this question WT and *Tnfr1/2*$^{-/-}$ mice were lethally irradiated and reconstituted with WT bone marrow cells to generate WT/WT and WT/*Tnfr1/2*$^{-/-}$ chimeras. Upon reconstitution both groups of chimeric mice received an IP injection of Zymosan. We found that reconstitution of *Tnfr1/2*$^{-/-}$ mice with WT bone marrow was not sufficient to rescue FALC formation upon inflammation at day 3 post-injection. Inflammation led to an enlargement of FALCs and recruitment of myeloid cells but failed to induce the formation of more clusters as it did in the control WT bone marrow chimeras (Fig. 5b). Thus, our data indicate that radiation resistant stromal cells respond to TNF and induce FALC formation.

We next determined the cellular origin of TNF, using mouse strains with specific deletion of *Tnf* in either $CD4^+$ T cells (T-TNF, CD4-Cre), B cells (B-TNF, CD19-Cre) or macrophages/neutrophils (M-TNF, LysM-Cre)[45]. Specific ablation of *Tnf* in T and B cells did not impair the induction of cluster formation upon inflammation as seen by the 3- and 2-fold increase in cluster numbers observed in T-TNF and B-TNF mice respectively (Fig. 5c). In contrast, loss of *Tnf* expression by neutrophils and macrophages in M-TNF mice

resulted in the absence of new FALC formation following Zymosan injection, even though CD11b^{+} myeloid cells were recruited to the clusters (Fig 5c). We then analysed by intra-cellular flow-cytometric staining the cellular origin of TNF in the mesenteries following Zymosan injection. As expected most of TNF^{+} cells were of myeloid origin (data not shown) with 40% of F4/80^{+} macrophages and Ly6C^{high}F4/80^{-} monocytes displaying intra-cellular TNF expression (Fig. 5d). Once correlated to their cell number, macrophages represented 60% of all TNF^{+} myeloid cells in the mesenteries (Fig. 5d).

Taken together, these results demonstrate the importance of TNFR1/2 signalling in stromal cells for de novo formation of FALCs upon inflammation and that macrophages are a key source of TNF.

CD1d-restricted NKT cells are necessary for FALC formation upon inflammation.

Given the prevalence of B cells in FALCs, we evaluated their role in the formation of these clusters upon inflammation. To do so, we analysed the effect of IP injection of Zymosan in *Rag2*$^{-/-}$ mice, lacking T and B cells, and in µ*MT*$^{-/-}$ mice that are deficient in B cells. Unexpectedly, we found that B cells were not involved in FALC formation upon inflammation as shown by the three-fold increase in their number (Fig. 6a) and the recruitment of CD11b^{+} myeloid cells after inflammation in these mice (Fig. 6b). However, peritoneal inflammation failed to induce cluster formation in *Rag2*$^{-/-}$ mice indicating that a T cell subset was necessary for neo-formation of FALCs upon inflammation (Fig. 6a). This result was confirmed by the absence of new cluster formation after Zymosan injection, in *CD3*ε$^{tg26-/-}$ mice, in which the development of T, NK and NKT cells is blocked. In both *Rag2*$^{-/-}$ and *CD3*ε$^{tg26-/-}$ mice, inflammation induced a normal recruitment of myeloid cells in FALCs (Fig. 6a-b).

We further characterised the role of T cells in FALC formation upon inflammation by examining the effect of Zymosan injection in *Tcr*δ$^{-/-}$ mice, which lack γδ T cells. Remarkably, Zymosan induced a five-fold increase in FALC numbers in *Tcr*δ$^{-/-}$ mice compared to a two-fold increase in WT mice, indicating that γδ T cells are not necessary for FALC formation following inflammation. In contrast, γδ T cells might have a regulatory role in the formation of the clusters (Fig. 6a-b).

We next assessed the role of CD1d-restricted Natural Killer T (NKT) cells in inflammation-induced FALC formation. We found that the number of FALCs was decreased two-fold in *Cd1d*$^{-/-}$ mice compared to WT mice and that injection of Zymosan failed to induce cluster formation at day 3 post-injection in this mutant strain (Fig. 6a-b).

This result indicated an important role for NKT cells in FALC formation during homeostasis and upon inflammation.

Activation of iNKT cells induces FALCs formation

NKT cells recognise lipid-based antigen presented by CD1d. The best characterised NKT cell population is Type I CD1d-restricted NKT cells, also known as invariant NKT cell (iNKT), in reference to their invariant TCR α-chain usage (Vα14-Jα18 in mice). Type I NKT cells recognise and strongly respond to the synthetic glycolipid α-Galactosylceramide (αGalCer) presented on CD1d[28]. A number of studies have recently described the presence of iNKT cells in adipose tissue and their role in regulation of metabolism[46–50]. Flow cytometric analysis of Type I NKT cells confirmed that these cells were particularly enriched in adipose tissue representing up to 6% of all lymphocytes, compared to the spleen (up to 0.3%) or the mLN (up to 0.1%) (Fig. 7a). Since it is not possible to detect iNKT cells by immuno-fluorescence, we transferred CFSE-labelled iNKT into WT mice and showed that these cells were indeed recruited to FALCs (Fig. 7b).

We next tested the effect of iNKT cell activation on FALC formation by IP injection of αGalCer into WT mice and showed a two-fold increase in the number of clusters in animals injected with this glycolipid compared to control littermates that received vehicle. This demonstrated that direct TCR activation of iNKT cells was sufficient to induce cluster formation (Fig. 7c). Since we found that Zymosan-induced FALC formation was dependent on TNFR1/2 signalling, we assessed whether these pathways were also required for cluster formation following iNKT cell activation via αGalCer. We showed that FALC formation upon αGalCer injection was indeed abrogated in *Tnfr1/2*$^{-/-}$ mice, indicating the need for signalling through these receptors (Fig. 7d). While IP injection of αGalCer induced a marked increase in the levels of CD69 and CD25 on iNKT cells, Zymosan did not appear to have a similar effect (data not shown).

To test whether iNKT cells were sufficient to rescue inflammation-induced FALC formation in *Rag2*$^{-/-}$ mice, we transferred sorted splenic iNKT cells by IP injection in these mice, 24 hours before immunisation with Zymosan. Our results showed that only mice that received iNKT cells responded to the Zymosan injection by presenting with an increase in FALC numbers (Fig. 7e). In contrast, mice receiving CD3^{high} cells, that do not contain NKT cells, were not able to rescue FALC formation following inflammation.

We next tested the effect of the selective loss of Type I iNKT cells on the formation of FALCs upon Zymosan-induced inflammation. We found that FALC numbers were

normally increased two-fold in *Jα18*$^{-/-}$ mice following Zymosan injection (Fig. 7f) indicating that Type I iNKT cells were not absolutely required for formation of these clusters. Taken together, these results indicate that even though Type I iNKT cells were sufficient to restore cluster formation in *Rag2*$^{-/-}$ mice, the function of Type I and Type II iNKT cells appear to be overlapping during inflammation-induced FALC formation.

Formation of FALCs upon inflammation is dependent on IL-4Rα signalling

Upon activation, iNKT cells produce very rapidly large amounts of Th-1 and/or Th-2 type cytokines, that link innate and adaptive immune responses and play important immuno-regulatory functions[28]. To understand the involvement of Th1 and Th2 cytokines in inflammation-induced FALC formation, we tested the effect of Zymosan-induced inflammation in mice deficient in either of these cytokines. We found that FALC formation induced by the injection of Zymosan was not impaired in *Ifnγ*$^{-/-}$ mice, indicating that the prototypic Th-1 type cytokine does not appear to be required for this process (Supp. Fig 5).

In contrast, Zymosan injections failed to induce formation of new clusters at day 3 post-injection in *Il4rα*$^{-/-}$ mice, where signalling by IL-4 and IL-13 is impaired, while the BALB/c WT mice responded with a two-fold increase in the number of FALCs (Fig. 8a-b). Additionally, we noticed that FALC numbers were two-times higher in the BALB/c mouse strain compared to the C57BL/6J strain, suggesting that the Th2 bias shown in the former during immune responses contributes to the higher number of FALCs found in this genetic background. To determine the respective contribution of IL-4 and IL-13, we assessed the formation of FALCs upon inflammation in the *Il4*$^{-/-}$ and *Il13*$^{-/-}$ mouse strains. We found that Zymosan injection led to the formation of new clusters in both mutant strains, suggesting that IL-4 and IL-13 were exerting redundant functions in FALC formation upon inflammation in the BALB/c background (Fig. 8a-b). However, IL-13 played a critical role in inflammation induced FALC formation in the C57BL/6J background as shown by the absence of cluster formation in *Il13*$^{-/-}$ mice at day 3 post-injection (Fig. 8c). To test whether IL-13 produced by iNKT cells was sufficient to rescue inflammation-induced FALC formation in *Il13*$^{-/-}$ mice, we transferred sorted splenic iNKT cells into these mice, 24 hours before immunisation with Zymosan. We found that IL-13-sufficient iNKT cells induced a slight increase in FALC numbers in *Il13*$^{-/-}$ mice but this did not reach statistical significance (Fig. 8c). These results indicate that IL-13 contributes to inflammation-induced FALC

formation, but that iNKT production of this cytokine is not sufficient for this process and an additional source of IL-13 may be required.

We finally assessed the role of IL-4Rα signalling in the formation of FALCs driven by direct iNKT cell activation via αGalCer injection. αGalCer injection failed to induce FALCs formation in *Il4rα*$^{-/-}$ mice indicating that formation of FALCs through direct activation of iNKT cells also required IL-4Rα signalling (Fig. 8d).

IL-4c induces a partial rescue of inflamation-induced FALC formation in the absence of TNF signalling

Our results showed that TNF- and IL-4-signals are necessary for inflammation-induced FALC formation. To get insight into the levels of interaction of the signals induced by these cytokines, we performed a serie of combinatorial and rescue experiments. As shown in Supp. Fig. 6a, injection of TNF and IL-4 complex (IL-4c) on their own or together was not sufficient to induce cluster formation, indicating that other factors were involved in this process. Next we tested whether IP injection of TNF could rescue Zymosan-induced FALC formation in *Il-4r*$^{-/-}$ mice. Our results show no significant increase in the number of clusters induced by Zymosan in this mutant strain. In contrast, IP injection of IL-4c in *Tnfr1/2*$^{-/-}$ mice induced a small but significant increase in the number of Zymosan-induced FALCs, indicating that IL-4 could partially rescue cluster formation in *Tnfr1/2*$^{-/-}$ mice and suggesting that IL-4 may act downstream of TNFR1/2 signalling (Supp. Fig. 6b).

DISCUSSION

In this report we defined the requirements for the formation of a new type of lymphoid tissue called Fat Associated Lymphoid Clusters. These non-conventional lymphoid clusters developed in close association with VATs of the peritoneal and pleural cavities. We showed that in the peritoneal cavity, mesenteric FALCs and omental milky spots accounted for the quasi-totality of the lymphoid clusters associated with adipose tissue. We uncovered the previously unappreciated abundance of FALCs in the pericardium and mediastinum of the pleural cavity where the density of lymphoid clusters approached the levels found in the omentum. Microscopic analysis of FALCs revealed a high B1 cell content with no apparent B and T cell segregation, comparable to what has been reported previously for the milky spots of the omentum[12]. FALCs expressed high levels of CXCL13 required for efficient recruitment of B cells, which upon immune challenge with T-dependent or -independent antigens actively proliferate, undergo differentiation towards plasma cells or GC cells in these clusters. The function of FALCs and milky spots are probably overlapping in the peritoneal cavity, but FALCs contained in the mediastinal and the pericardial fat are likely to be the main sites for the organization of immune responses and for retention of B1 cells by CXCL13 in the pleural cavity.

FALC development in mice was constitutive and its initiation coincided with weaning. Establishment of a normal number of FALCs in adult mice was dependent on TNFR1/2 signalling and colonisation by commensal flora suggesting a role for Pattern Recognition Receptors. FALCs were totally absent in *Rag2*$^{-/-}\gamma c^{-/-}$ mice and immunofluorescence and flow-cytometric analysis in *Rag2*$^{-/-}$ mice indicated that cells present in the clusters in absence of T and B cells were ILCs. Importantly, FALC formation was independent of the presence of LTi cells and other ILC3 cells as well of LTα-LTβR-signalling which resembles the formation of nasal associated lymphoid tissues (NALT)[51]. Although we have developed a number of ILC2-deficient mouse strains[52, 53] these mice still have residual numbers of ILC2-like cells and we have not been able to show categorically whether these cells play a role in FALC formation (data not shown).

Peritoneal inflammation induced a rapid neo-formation of a large number of FALCs reaching a two- to three-fold increase compared to the number of clusters present in resting conditions. This effect was dependent on TNF expression by myeloid cells and TNFR1/2 signaling on stromal cells. We further showed that most TNF producing cells in the mesenteries are macrophages. In addition to the innate requirement for TNF^{+} myeloid cells, neo-formation of FALCs necessitated the activation of iNKT cells and signalling

through the IL4Rα. Our data also demonstrated that IL-13 contributed to inflammation-induced FALC formation. Interestingly, triggering of iNKT cells through TCR ligation was sufficient to induce formation of FALC that was also dependent on TNFR1/2 and IL-4Rα signalling. Therefore, induction of FALC formation seems to require both an inflammatory signal, delivered by TNF, and a Th2/Resolution signal transduced by IL-4Rα. The fact that IL-4c can partially rescue FALCs formation upon Zymosan injection indicates that IL-4Rα signals could be acting downstream of the TNF receptors. How FALC formation is timed with the iniation of the resolution of inflammation and whether FALCs play a role in the resolution phase remains to be investigated.

We thus propose a multistep model where FALC development starts after birth with the clustering of immune cells in VAT (See model Fig. 8e). Colonization by the microbiota induces TNF that upon engagement of the TNF receptors results in the expression of IL-4Rα ligands that are required for the expansion of the number of FALCs to the levels seen in adult mice. This model is in agreement with a recent report showing that TNF-signalling induces IL-13 expression on adipocytes during diet-induced obesity[54]. Expression of CXCL13 by stromal cells results in the recruitment of B cells. Peritoneal inflammation induces a rapid increase in the size and number of FALCs that is dependent on TNF-R signalling on stromal cells as well as IL-4R mediated signals and NKT cell activation. Moreover, FALCs support Ag-specific B cell recruitment, proliferation and differentiation. ILC2 express high levels of IL5 that might drive the proliferation of B1 cells in the clusters[55]. Coupling of inflammation and rapid FALC formation provide a platform to link innate and adaptive immune responses that support rapid B cell proliferation and natural antibody secretion in the body cavities following infection.

We and others have recently shown that adipose tissues constitute an important reservoir of stem cells for the formation of lymphoid stroma in LNs during development[22, 56] and immune responses[57]. It is thus conceivable that FALC stromal cells originate from adipose tissue stem cells or peri-vascular cells, as has been recently shown for FDCs[22]. FALC stromal cells expressed high levels of CXCL13 but were negative for CD21/35.

Different populations of macrophages, Treg cells, NKT cells, B cells, ILCs and eosinophils have been described to be present in the peritoneal cavity and their metabolic regulatory functions are increasingly studied[58–60]. The relation between these cell populations and FALCs will require further studies to be elucidated.

This work constitutes the first report of NKT cells having a lymphoid organogenic activity. Not only were NKT cells necessary for the formation of FALCs during inflammation, but also their sole activation was sufficient to induce neo-formation of

clusters. A number of studies have recently highlighted the role of NKT cells in the regulation of adipose tissue metabolism in normal nutrient homeostasis and during obesity[46–50]. Whether the metabolic activity of NKT cells is linked to their capacity to induce FALC formation and alter the homeostasis of other hematopoietic cells present in adipose tissues remains to be investigated.

MATERIALS AND METHODS

Mice

C57BL/6J (H-2^b), *Ltβr*$^{-/-}$, *Ltα*$^{-/-}$, *Rorc*$^{-/-}$, *Rag2*$^{-/-}$, *Rag2*$^{-/-}$*γc*$^{-/-}$, *Tnfr1/2*$^{-/-}$, *Tnf*$^{+/\Delta ARE36}$, and *Eyfp-Rosa 26*[55], *Plt/plt*, *Ccr7*$^{-/-}$, *Cxcr5*$^{-/-}$, QM/QM (IgH$^{NP/NP}$ Igκ$^{-/-}$), QMxB6 (IgH$^{NP/wt}$ Igκ$^{-/wt}$), QM/QM (IgH$^{NP/NP}$ Igκ$^{-/-}$)EYFP$^+$, Cg1-CrexQMmTmG (IgH$^{NP/C_\gamma 1Cre}$ Igκ$^{-/-}$ mTmG$^{+/wt}$), Cd3ε$^{tg26-/-}$, Cd1d$^{-/-}$, TNF$^{fl/fl}$LysM-Cre (M-TNF)[45], TNF$^{fl/fl}$CD4-Cre (T-TNF)[45] or TNF$^{fl/fl}$CD19-Cre (B-TNF)[45], Vα14 transgenic, *Ifnγ*$^{-/-}$ (on C57BL/6J background), *Il4*$^{-/-}$ (on BALB/c background) and BALB/c (H-2^d) mice were bred and maintained under specific pathogen-free conditions. *Il13*$^{-/-}$*, and Il4rα*$^{-/-}$ mice were used in C57BL/6J or BALB/c background for experiments as indicated. Germ-free C57BL/6J mice were obtained from the Institut Pasteur, Paris, France. Bone marrow chimeras were generated after irradiation of C57BL/6J and *Tnfr1/2*$^{-/-}$ mice and reconstitution with bone marrow from C57BL/6J. All experiments in this report were performed according to UK Home Office and local ethics committee regulations.

Immunization and peritoneal cavity inflammation

QM/QM (IgH$^{NP/NP}$ Igκ$^{-/-}$), QMxB6 (QM$^{IgH/wt}$ Igκ$^{-/wt}$), and Cγ1-CrexQMmTmG mice were immunised by IP injection of 30 mg NP40-Ficoll per mouse (Biosearch Technologies, Novato, CA, USA). B cell activation from mesenteries, spleen, mLN and peritoneal cavity lavage was assessed 24 hours later (QM/QM mice) or 4 days latter (QMxB6 and Cγ1-CrexQMmTmG mice) by flow cytometry and ELISpot. IgG1 switching in the mesenteries was visualized at day 4 by wholemount stereo-microscopy. For the cell transfer experiment, 2.10^6 peritoneal lavage cells from QM/EYFP$^+$ (QM/QM (IgH$^{NP/NP}$ Igκ$^{-/-}$)EYFP$^+$) mice were transferred IP into recipient C57BL/6J mice, before immunization with NP-OVA (50 mg) precipitated with Alum on the next day. B cell activation was assessed at day 8 in the mesenteries, spleen and mLN. For the PE immunization experiment, C57BL/6J mice were immunized IP with Phycoerythrin (PE) (50 mg) and B cell activation was analysed at day 8-9 in the mesenteries, spleen and mLN. Peritoneal cavity inflammation was induced by IP injection of 1mg Zymosan (Sigma). 72 hours later, B cell activation was assessed by flow cytometry, FALC number and composition were assessed by whole mount fluorescence staining and confocal analysis. Treatment of mice with IL-4c was performed as previously described[61]. IL-4c consisted of a 2:1 molar ratio of recombinant mouse IL-4 (Peprotech) and anti-IL-4 mAb (clone 11B11;BioXcell). Mice were injected i.p. with IL-4c

containing 5 μg of IL-4 and 25 μg of 11B11, or PBS vehicle control on days 0 and 2. For co-administration experiments with Zymosan, mice were given 1mg Zymosan on day 0 with IL-4c on day 0 and day 2. Mice were treated with 1ug TNF (Peprotech) or PBS control on day 0 and day 2. For co-administration experiment with IL-4c, mice were treated with IL-4c and TNF on day 0 and day 4. For co-administration experiment with Zymosan, mice were given 1mg Zymosan on day 0 and TNF on day 0 and day 2. In all experiments with IL-4c and TNF, analysis of the mesenteries was performed on day 4.

Cell isolation and cell sorting

For flow cytometric analysis of the mesenteries, tissues were digested for 30 minutes in RPMI containing 1% fetal calf serum and 1mg/ml Collagenase D (Roche) at 37°C on constant agitation (110 rpm). Tissue suspensions were filtered was filtered through 40μm cell strainers before staining. Peritoneal cavity lavage was performed by injection of 5ml cold PBS in the peritoneal cavity. Isolation of splenic iNKT cells and $CD3^{high}$ T cells was performed via MoFlow (Dako Cytomation) cell sorting. 500000 cells (purity> 98%) were injected in the peritoneal cavity of *Rag2*$^{-/-}$, 12 hours before induction of peritoneal cavity inflammation. Mesenteries were analyzed for cluster formation 72 hours later. For CFSE labeling, iNKT cells were cell-sorted from the spleen of Vα14 transgenic mice in which 30-40% of all cells are positive for αGalCer-loaded CD1d tetramers and were incubated for 10 minutes at RT with 5μM CFSE (eBiosciences) according to manufacturer indications prior to IP injection. CD1d-PBS57 loaded tetramers were kindly provided by the National Institutes of Health Tetramer Facility (Atlanta GA, USA).

FALC isolation

Clusters were isolated using a fluorescent stereomicroscope from unfixed mesenteries of $Eyfp^{+}$ mice in which the bright $EYFP^{+}$ lymphoid aggregates could be visualised without prior fluorescent staining. Isolated clusters were used for qPCR analysis.

Antibodies and reagents for flow cytometry

Antibodies and reagents used for flow cytometry are listed in Supplementary Table 1. Single cell suspensions were stained with primary conjugated antibodies followed by secondary antibodies. NP-specific B cells were detected with NP-PE, added with the primary antibody staining mix. iNKT cells were detected with CD1d tetramer conjugated with APC preloaded with PBS-57 (an analog of α-GalCer). CD1d-PBS-57-APC was also

added to the primary antibody staining mix. For Ki67 nuclear staining, cells were fixed and permeabilized with the Foxp3 Fixation/Permeabilization kit (eBiosciences). Flow cytometric analysis was performed using Cyan (BD Biosciences) with forward/side scatter gates set to exclude non-viable cells. Data were analyzed with FlowJo software (version 8.8.3, Tree Star).

ELISpots

$2.5x10^5$ cells from the mesenteries or spleen were seeded into precoated NP_{15}-BSA (5µg/ml)- nitrocellulose microtiter plates. After 24h culture the plates were washed and incubated in isotype specific alkaline phosphatase-conjugated antibody IgM-AP1/ IgG-AP1 (SouthernBiotech) diluted in PBS-1%BSA for 2 hours at RT and colorated using Fast BCIP/NBT alkaline phosphatase substrate (Sigma). Spots were counted using an AID ELISpot reader (Autoimmun Diagnostika GmbH, Strassburg, Germany) with Eli4 software (Autoimmun Diagnostika GmbH).

RT-PCR and real-time RT-PCR

mRNAs were isolated from tissues using the RNeasy mini kit (Qiagen), and reverse transcription was performed using the High capacity reverse transcription cDNA synthesis kit (Applied Biosystems). Quantitative RT-PCR was performed using primers and probes from Applied Biosystems for Cxcl13 (Mm00444533_m1), Ccl21 (Mm03646971_gH), Ccl19 (Mm00839967_g1), Tnf (Mm00443258_m1), LTβ (Mm00434774_g1) and Il-7 (Mm01295803_m1) using ABI PRISM 7900HT instrument. The means of duplicate of the ratio of the gene of interest to β-actin are shown.

Immunofluorescence staining

After dissection, whole mesenteries were fixed in PBS 4%PFA for 1 hour at 4°C, permeabilized in PBS 1%Triton for 30 minutes at room temperature (RT). Tissues were then stained with primary antibodies for 1 hour at RT on constant slow agitation. After wash, tissues were stained with secondary antibodies for 30 minutes at RT. Antibodies used are listed in Supplementary Table 1. Tissues were mounted using Vectashield mounting medium (Vector Laboratories).

Image acquisition and analysis of confocal images

Confocal images were acquired using a Zeiss LSM 510 laser scanning confocal head with

a Zeiss Axio Imager Z1 microscope. For all analysis of clusters a minimum of 12 clusters were analysed from 4 mice of each group and pooled from 2 independent experiments.

Statistical analysis

Statistical significance was determined for all analysis with a Mann-Whitney non parametric two-tailed test.

ACKNOWLEDGMENTS

We are grateful to the personnel in BMSU for taking care of our animal colonies. We want to thank Eric Jenkinson for continuous support. We are thankful to Graham Anderson, Peter Lane, and Antal Rot for comments on the manuscript. We are also thankful to Chris Buckley for facilitating animal procedures and to Roger Bird for cell sorting. We are indebted to Klaus Pfeffer, Gerard Eberl, Daniela Finke, and Andreas Diefenbach for providing mouse strains and reagents. CD1d-PBS57 loaded tetramers were kindly provided by the National Institutes of Health Tetramer Facility (Atlanta GA, USA).

This work was supported by the EU FP7 integrated project INFLACARE and a BBSRC grant (BB/K004900/1) to J. Caamaño. The work in A. McKenzie laboratory was supported by the American Asthma Foundation, UK-MRC and the Wellcome Trust (grant number 100963/Z/13/Z). M. Veldhoen laboratory was supported by the BBSRC institute synergy programme grant, and ERC grant (280307). Work in Sergei Nedospasov laboratory was supported by DFG (NE1466/2-1) and a grant from Russian Science Foundation (14-50-00060) and grant to A.A.K from RFBR (13-04-40268). G. Kollias laboratory was supported by ERC grant 340217 - MCs_inTEST. S. Nayar was the recipient of an MRC DTA PhD studentship. LHJ was funded by the UK-MRC (MRC/K01207X/1). YL was supported by a MB/PhD scholarship from the Agency of Science, Technology and Research (A*STAR). KMT, YZ and JM were supported by a granted through the Lifelong Health and Wellbeing cross council initiative (Topjabs G1001390).

Author Contributions: C.B., N-T.L., J.A.W., A.A.K., Y.L., K.N., Y.Z., S.N, L.J. and J.C. designed and performed the research, collected and analyzed the data. A.F-L., A.M., J.M., F.B., G.B., K.M., J.A., M.G., G.K., A.F.C., D.W., K.M.T., N.D.J., M.V., S.A.N. and A.N.J.M. facilitated the research. C.B. and J.C. wrote the manuscript.

Author Information: The authors declare that there is no conflict of financial interest. Correspondence and request for materials should be addressed to C. Bénézech (c.benezech@staffmail.ed.ac.uk) or J. H. Caamaño (j.caamano@bham.ac.uk).

FIGURE LEGENDS

Figure 1: Distribution of FALCs in VAT

(**a**) Whole mount immunofluorescence staining of the mesenteries allowing visualisation of $CD45^+$ FALCs (green) (**b**) Density of hematopoietic clusters (number of clusters/g adipose tissue) in the main fat deposits of the peritoneal (omental (n=8 mice), gonadal (n=7) and mesenteric (n=6) adipose tissues) and pleural cavities (mediastinal (n=13) and pericardial (n=8) adipose tissues) and in the subcutaneous fat (n=7). Data points and mean shown. Data pooled from two independent expts. (**c**) Percentages of clusters found in each fat deposit relative to the total number of clusters found in the peritoneal or pleural cavities. (**d**) Whole mount immunofluorescence staining showing a mesenteric FALC with $CD11b^+$ myeloid cells (blue), $CD45^+$ hematopoietic cells (green), IgM^+ B cells (red), and $CD4^+$ T cells (white). (**e**) Whole mount immunofluorescence staining showing a mesenteric FALC with $CD45^+$ hematopoietic cells (green), $CD31^+$ blood endothelial cells (red) and Lyve-1^+ cells (blue). Scale bar 50 µm. (**f**) Enumeration of the mesenteric clusters of newborns and animals aged between 1 and 32 weeks (n=5, 5, 5, 5, 7, 18, 7, 7 mice per group). Data points and mean shown.

Figure 2: CXCL13 expression by FALC stromal cells is necessary for B cell recruitment

(**a**) Real-time PCR analysis of the indicated mRNA in LNs, mesenteric FALCs and adjacent fat (n=5, 4, 5). Mann-Whitney nonparametric two-tailed test between FALCs and fat *Cxcl13* p=0.0159, *Tnf* p=0.0286, *Ccl21* p=0.1143, *Ltb* p=0.0079, *Ccl19* p=0.2857, *Il7* p=0.0286. (**b-c**) Numbers of mesenteric clusters in *WT*, *Plt/plt*, $Ccr7^{-/-}$, and $Cxcr5^{-/-}$ mice (n=7, 6, 6, 6 mice per group), (**b**) and whole mount immunofluorescence staining showing FALCs with $CD11b^+$ myeloid cells (blue), $CD45^+$ hematopoietic cells (green), IgM^+ B cells (red), and $CD4^+$ T cells (white) (**c**) in the indicated mouse strains. (**d**) Whole mount immunofluorescence staining showing mesenteric FALCs in the indicated mouse strains with $CD45^+$ hematopoietic cells (green), and $CXCL13^+$ stromal cells (red). Scale bar 50 µm. $*p < 0.05$, $**p < 0.01$, $***p < 0.001$ and $****p < 0.0001$, ns not significant.

Figure 3: B cell activation and differentiation in FALCs upon peritoneal immune challenge

(**a**) NP-specific IgM and IgG ELISpot assays and number of AFC on isolated FALCs and spleen cells after NP-Ficoll IP immunisation of QMxB6 mice. Data correspond to PBS and

NP-Ficoll treated mice (n=12,12) pooled from 2 independent experiments (n=9 FALCs and 12 spleen). Mann-Whitney nonparametric two-tailed test between PBS and NP-Ficoll immunised mice, FALCs IgM p=0.0037, spleen IgM p<0.0001, FALCs IgG p=0.0275 and spleen IgG p<0.0001. (**b**) Whole mount immunofluorescence staining of the mesenteries of Cg1-CrexQMmTmG mice that were immunised with either PBS (all cells red) or NP-Ficoll that results in the generation of IgG1$^+$-switched FALC B cells (green). (**c-e**) Peritoneal lavage cells from QM/QM EYFP$^{+/-}$ mice were transferred by intravenous (IV) injection into C57BL/6J mice 24 hours before immunisation with Alum-precipitated NP-OVA. (**d**) Flow-cytometric analysis of cells isolated from the mesenteries, spleen and mLN of PBS and NP-OVA-immunised mice showing the percentage of EYFP$^+$CD19$^+$ NP-specific B cells in live CD45$^+$ gate (upper row) and percentage of CD38$^-$GL7$^+$ GC B cells in EYFP$^+$CD19$^+$ NP-specific B cells gate (lower row). (**e**) Quantification of the cell number of NP-specific B cells (left column) and NP-specific GC B cells (right column). Data correspond to PBS and NP-OVA treated mice (n=5, 6) pooled from 2 independent experiments. Mann-Whitney nonparametric two-tailed test between PBS and NP-OVA treated mice, percentages of NP$^+$ B cells in the mesenteries p=0.0022, spleen p= 0.0455, mLN p= 0.0043, number of NP$^+$ B cells in the mesenteries p= 0.0079, spleen p=0.0317, mLN p=0.0079, percentages of NP$^+$ GC B cells in the mesenteries p= 0.0022, spleen p=0.0022, mLN p=0.0043 and number of NP$^+$ GC B cells in the mesenteries p=0.0043, spleen p=0.0043, mLN p=0.0043. (**f-h**) C57BL/6J mice were immunised IP with Alum precipitated-PE. (**g**) Flow-cytometric analysis of the mesenteries of naïve and PE immunised mice showing percentages of PE$^+$CD19$^+$ B cells in live CD45$^+$ gate (upper row), and CD38$^-$GL7$^+$ GC B cells in PE$^+$CD19$^+$ gate (lower row). (**h**) Quantification of the cell number of PE$^+$ GC B cells. Data correspond to PBS and PE/Alum immunised mice (n=6, 7) pooled from 2 independent experiments. Mann-Whitney nonparametric two-tailed test between PBS and PE/Alum immunised mice, percentages of PE$^+$ GC B cells in the mesenteries p=0.0043, spleen p= 0.0012, mLN p= 0.0012, number of PE$^+$ GC B cells in the mesenteries p= 0.0043, spleen p=0.0012, mLN p=0.0012 (**h**). *p < 0.05, **p < 0.01, ***p< 0.001 and ****p <0.0001.

Figure 4: Factors controlling the development of FALCs

(**a**) Number of mesenteric clusters in the indicated knockout mouse strains. Data correspond to WT, *Ltβr*$^{-/-}$, *Ltα*$^{-/-}$, *Rorc*$^{-/-}$, *Rag2*$^{-/-}$, *Rag2*$^{-/-}$*γc*$^{-/-}$, germ free (*GF*), *Tnfr1/2*$^{-/-}$ and *Tnf*$^{+/\Delta ARE}$ mice pooled from at least 2 independent experiments (n=19, 13, 8, 7, 10, 7, 9, 9, 9 mice per group). Mann-Whitney nonparametric two-tailed test between WT and *Rag2*$^{-/-}$

$\gamma c^{-/-}$ p< 0.0001, WT and *GF p<0.0001*, WT and *Tnfr1/2*$^{-/-}$ p=0.0002, WT and *Tnf*$^{+/\Delta ARE}$ p<0.0001 (**b**) Whole mount immunofluorescence staining showing FALCs with CD11b$^+$ myeloid cells (blue), CD45$^+$ hematopoietic cells (green), IgM$^+$ B cells (red), and CD4$^+$ T cells (white) in the indicated mouse strains. (**c-e**) Microphotographs of the mesenteries (**c**), number of clusters (**d**) and whole mount immunofluorescence staining as in b (**e**) after PBS or Zymosan injection (n=8, 9). Data pooled from 2 independent experiments. Mann-Whitney nonparametric two-tailed test p<0.0001. Scale bar 50 µm. **p* <0.05, ***p* <0.01, ****p*<0.001****, *p* <0.0001.

Figure 5: TNF is required for FALC formation upon inflammation

(**a**) Number of clusters found in the mesenteries of *Tnfr1/2*$^{-/-}$ mice and whole mount immunofluorescence staining showing FALCs with CD11b$^+$ myeloid cells (blue), CD45$^+$ hematopoietic cells (green), IgM$^+$ B cells (red), and CD4$^+$ T cells (white) 72 hours after PBS or Zymosan injection. Data pooled from 2 independent experiments (n=6, 6). Mann-Whitney nonparametric two-tailed test p=0.2424. (**b**) Number of clusters present in the mesenteries of WT and *Tnfr1/2*$^{-/-}$ mice reconstituted with WT bone marrow and whole mount immunofluorescence staining as in **a** after PBS or Zymosan injection. Data correspond to WT BM into WT mice (n=5, 5) and WT BM into *Tnfr1/2*$^{-/-}$ mice (n=6, 6) per group pooled from 2 independent experiments. Mann-Whitney nonparametric two-tailed test, WT BM into WT mice p=0.0079, and WT BM into *Tnfr1/2*$^{-/-}$ mice p=0.1688. (**c**) Enumeration of clusters in the mesenteries of the indicated mutant mouse strains and whole mount immunofluorescence as in **a** after PBS or Zymosan injection. Data correspond to WT mice (n=7, 7), *T-Tnf*$^{-/-}$ (n=6, 8), *B-Tnf*$^{-/-}$ (n=4, 6) and *M-Tnf*$^{-/-}$ (n=8, 13) mice in the control and treated group pooled from 2 independent experiments. Mann-Whitney nonparametric two-tailed test WT p=0.0006, *T-Tnf*$^{-/-}$ p=0.0007, *B-Tnf*$^{-/-}$ p=0.0048 and *M-Tnf*$^{-/-}$ p=0.2156. Scale bar 50 µm. (**d**) Flow-cytometric analysis showing TNF intra-cellular staining 2 hours post Zymosan injection in mesenteric eosinophils (gated as CD45$^+$CD11b$^+$SSC^{high}Siglec-F$^+$), neutrophils (gated as CD45$^+$CD11b$^+$Siglec-F$^-$Ly6-G^{high}), macrophages (gated as CD45$^+$CD11b$^+$Siglec-F$^-$F4/80$^+$) and monocytes (gated as CD45$^+$CD11b$^+$Siglec-F$^-$F4/80$^-$Ly6-c^{high}). Quantification of the percentages of TNF$^+$ cells after Zymosan in myeloid subsets is shown in bar chart. Data correspond to WT mice in the control and treated group (n=8, 8) pooled from 2 independent experiments. Mann-Whitney nonparametric two-tailed test, eosinophils p=0.1593, neutrophils p=0.3935, macrophages p=0.0002 and monocytes p=0.0002. The distribution of TNF$^+$ myeloid cells in the different subsets is shown in the pie chart. ***p* <0.01, ****p*<0.001.

Figure 6: CD1d restricted NKT cells are required for FALC formation

(**a-b**) Number of mesenteric clusters in the indicated mouse strains (**a**) and whole mount immunofluorescence staining showing FALCs with CD11b$^+$ myeloid cells (blue), CD45$^+$ hematopoietic cells (green), IgM$^+$ B cells (red), and CD4$^+$ T cells (white) 72 hours after PBS or Zymosan injection (**b**). Data correspond to *Rag2*$^{-/-}$ (n=6, 6), *μMT*$^{-/-}$ (n=5, 5), *CD3ε*$^{tg26-/-}$ (n=5, 5), TCRδ$^{-/-}$ (n=4, 6) and *Cd1d*$^{-/-}$ (n=5, 6) mice in the control and treated group pooled from 2 independent experiments. Mann-Whitney nonparametric two-tailed test, *Rag2*$^{-/-}$ p=0.5693, *μMT*$^{-/-}$ p=0.0025, *CD3ε*$^{tg26-/-}$ p=0.7857, TCRδ$^{-/-}$ p=0.0095 and *Cd1d*$^{-/-}$ p=0.5065. Scale bar 50 μm. ***p* <0.01, ns not significant.

Figure 7: iNKT cell activation induces FALC formation

(**a**) Flow cytometry of the mesenteries, spleen and mLN showing the percentage of CD3ε$^+$ CD1d-αGalCer tetramer$^+$ iNKT cells in the lymphocyte gate. Data are representative of 3 independent experiments (**b**) Whole mount immunofluorescence staining showing CFSE loaded iNKT cells (green) in mesenteric FALCs with CD11b$^+$ myeloid cells (blue) and IgM$^+$ B cells (red) 24 hours after transfer. Data representative of 4 mice in 2 independent experiments. (**c-d**) Numbers of mesenteric clusters and whole mount immunofluorescence staining showing FALCs with CD11b$^+$ myeloid cells (blue), CD45$^+$ hematopoietic cells (green), IgM$^+$ B cells (red), and CD4$^+$ T cells (white) 72 hours after vehicle or αGalCer injection. Data correspond to WT mice in the control and treated group (n=6, 9) pooled from 2 independent experiments (**c**) and *Tnfr1/2*$^{-/-}$ mice in the control and treated group (n=9, 7) pooled from 3 independent experiments (**d**). Mann-Whitney nonparametric two-tailed test, WT p=0.0004 and *Tnfr1/2*$^{-/-}$ p=0.2831. (**e**) Numbers of mesenteric clusters and whole mount immunofluorescence staining showing FALCs with CD11b$^+$ myeloid cells (blue) and CD45$^+$ hematopoietic cells (green) 72 hours after PBS or Zymosan injection in *Rag2*$^{-/-}$ mice (n=4, 5) and *Rag2*$^{-/-}$ mice transferred with high purity sorted CD3^{high} T cells or CD3ε$^+$ CD1d-αGalCer tetramer$^+$ iNKT cells (n=6, 5). Data pooled from 4 independent experiments. Mann-Whitney nonparametric two-tailed test p=0.0043. (**f**) Numbers of mesenteric clusters in *Jα18*$^{-/-}$ mice and whole mount immunofluorescence as in **c** 72 hours after PBS or Zymosan injection (n=7, 6). Data correspond pooled from 2 independent experiments. Mann-Whitney nonparametric two-tailed test p=0.0012. Scale bar 50 μm. ***p* < 0.01, ****p*< 0.001 and ns not significant.

Figure 8: Formation of FALCs is dependant on IL-4Rα signaling

(**a-b**) Numbers of mesenteric clusters in the indicated mouse strains (**a**) and whole mount immunofluorescence staining showing FALCs with $CD11b^+$ myeloid cells (blue), $CD45^+$ hematopoietic cells (green), IgM^+ B cells (red), and $CD4^+$ T cells (white) 72 hours after PBS or Zymosan injection. Data correspond to WT (n=7, 6), *Il4rα*$^{-/-}$ (n=5, 5), *Il4*$^{-/-}$ (n=5, 6), and *Il13*$^{-/-}$ mice (n=4, 6) in the control and treated group pooled from 2 independent experiments. Mann-Whitney nonparametric two-tailed test, WT p=0.0012, *Il4rα*$^{-/-}$ p=0.8016, *Il4*$^{-/-}$ p=0.0043, and *Il13*$^{-/-}$ mice p=0.0095. (**c**) Numbers of mesenteric clusters in *Il13*$^{-/-}$ mice and *Il13*$^{-/-}$ mice transferred with high purity sorted CD1d-αGalCer tetramer$^+$ iNKT cells or $CD3^{high}$ T cells 72 hours after PBS or Zymosan injection. Data correspond to *Il13*$^{-/-}$ control (n=7), injected with Zymosan (n=6), injected with Zymosan and transferred with iNKT cells (n=6) and injected with Zymosan and transferred with $CD3^{high}$ T cells (n=6) pooled from 2 independent experiments. Mann-Whitney nonparametric two-tailed test p=0.3625. Scale bar 50 µm. (**d**) Numbers of mesenteric clusters in C57Bl/6J and *Il4ra*$^{-/-}$ mice 72 hours after PBS or Zymosan injection. Data correspond to WT control (n=9) and treated (n=5) and *Il4rα*$^{-/-}$ control (n=7) and treated (n=5) pooled from 2 independent experiments. Mann-Whitney nonparametric two-tailed test, WT p=0.001 and *Il4rα*$^{-/-}$ p=0.2159. (**e**) Scheme representing the cellular and molecular interactions involved in FALC formation during normal development (blue arrow) and following inflammation (red arrow). $^{**}p < 0.01$, $^{***}p < 0.001$ and ns not significant.

Supplementary Figure legends

Supplementary Figure 1: FALC morphology

Whole mount immunofluorescence staining showing a representative array of FALCs harvested from the mesenteries of a single mouse with $CD11b^+$ myeloid cells (blue), $CD45^+$ hematopoietic cells (green), IgM^+ B cells (red), and $CD4^+$ T cells (white). Scale bar 50 µm.

Supplementary Figure 2: B cell activation in FALCs upon peritoneal immune challenge

(**a**) Flow cytometry of the mesenteries of QM/QM ($IgH^{NP/NP}$ $Ig\kappa^{-/-}$) mice 24 hours post PBS (left panel) and NP-Ficoll (right panel) IP injection. In the $CD45^+$ hematopoietic fraction, the different B cell subsets were identified according to the expression of CD19 and CD11b (first row), CD19 and CD5 (second row). The percentages of NP^+Ki67^+ cells in the B2 ($CD19^+CD11b^-CD5^-$), B1c ($CD19^+CD11b^-CD5^+$), B1a ($CD19^+CD11b^+CD5^+$) and B1b ($CD19^+CD11b^+CD5^-$) cell subsets are shown (third and forth row). Image representative of 2 independent experiments (n=6, 5). (**b**) Quantification of the percentage of NP^+Ki67^+ activated B cells in the mesenteries, PCL and spleen of QM/QM mice 24 hours after PBS or NP-Ficoll injections. Data are representative of 2 independent experiments (n=6, 5). Mann-Whitney nonparametric two-tailed test, B2 p=0.1905 and p=0.0079, B1c p=0.0159, p=0.0079, B1a p=0.0159, p=0.0079, B1b p=0.0159, p=0.0079. (**c**) Whole mount immunofluorescence staining showing FALCs from of QM/QM mice after PBS or NP-Ficoll injection with $CD11b^+$ myeloid cells (blue), $CD45^+$ hematopoietic cells (green) and IgM^+ B cells (red). Scale bar 50 µm. *p < 0.05, **p < 0.01, ***p< 0.001, ****p < 0.0001, and ns not significant.

Supplementary Figure 3: ILC2 in VAT and FALCs

(**a**) Flow cytometry of the mesenteries showing $CD45^+Lin^-c\text{-}kit^+Sca\text{-}1^+IL\text{-}7R\alpha^+$ ILC2 in WT (first row) and *Rag2*$^{-/-}$ (second row) mice (NK1.1 and CD4 present in Lin cocktail). (**b**) Flow cytometric analysis of the mesenteries showing $CD45^+Lin^-Sca\text{-}1^+NK1.1^-$ ILC2 and $CD45^+Lin^-Sca\text{-}1\text{-}^+NK1.1^+$ NK cells in *Rag2*$^{-/-}$ mice. (**c**) Whole mount immunofluorescence staining showing FALCs in *Rag2*$^{-/-}$ with $CD11b^+$ myeloid cells (blue) and $CD90^+$ ILC (green). Scale bar 50 µm.

Supplementary Figure 4: Myeloid cells are recruited to FALCs upon inflammation

(**a**) Whole mount immunofluorescence staining showing FALCs containing $CD11b^+$ myeloid cells (blue) and $Ly6C^+$ monocytes (first row, green), $Gr1^+$ granulocytes (second row, green) or $F4/80^+$ macrophages (third row, green) after Zymosan injection. Scale bar 50 µm.

Supplementary Figure 5: IFN-γ is not necessary for FALC formation upon inflammation

Number of clusters found in the mesenteries of *Ifnγ*$^{-/-}$ mice and whole mount immunofluorescence staining showing FALCs with $CD11b^+$ myeloid cells (blue), $CD45^+$ hematopoietic cells (green), IgM^+ B cells (red), and $CD4^+$ T cells (white) 72 hours after IP injection of PBS or Zymosan. Data corrrespond to control (n=6) and treated (n=4) mice pooled from 2 independent experiments. Mann-Whitney nonparametric two-tailed test, p=0.0095. Scale bar 50 µm. $^{**}p < 0.01$.

Supplementary Figure 6: IL-4c induces a partial rescue of inflamation-induced FALC formation in the absence of TNF signalling

(**a**) Number of clusters found in the mesenteries of *C57BL/6J* mice and whole mount immunofluorescence staining showing FALCs with $CD11b^+$ myeloid cells (blue), $CD45^+$ hematopoietic cells (green), IgM^+ B cells (red), and $CD4^+$ T cells (white) 4 days after PBS, TNF, IL-4c and both TNF and IL4c injections. Data correspond to control (n=6) and TNF (n=6), IL-4c (n=7) and TNF+IL-4c (n=7) treated mice, pooled from 2 independent experiments. Mann-Whitney nonparametric two-tailed test, PBS and TNF p=0.4248, PBS and IL-4c p=0.4156, PBS and TNF+IL-4c p= 0.7964. (**b**) Number of clusters found in the mesenteries of *C57BL/6J*, *Il4rα*$^{-/-}$ and *Tnfr1/2*$^{-/-}$ mice and whole mount immunofluorescence staining as in **a**, 4 days after PBS, Zymosan, Zymosan+TNF, and Zymosan+IL-4c injections. Data correspond to PBS (n=13), Zymosan (n=15) and Zymosan+TNF (n=9) treated WT mice pooled from 3 independent experiments, and to PBS (n=7), Zymosan (n=7) and Zymosan+TNF (n=8) treated *Il4rα*$^{-/-}$ mice pooled from 2 independent experiments, and to Zymosan (n=7) and Zymosan+IL-4c (n=7) treated *Tnfr1/2*$^{-/-}$ mice pooled from 2 independent experiments. Mann-Whitney nonparametric two-tailed test WT PBS and Zymosan p<0.0001, WT PBS and Zymosan+TNF p=0.0052, *Il4rα*$^{-/-}$ PBS and Zymosan p=0.0105, *Il4rα*$^{-/-}$ PBS and Zymosan+TNF p=0.0365, *Il4rα*$^{-/-}$ Zymosan and Zymosan+TNF p=0.7574, and *Tnfr1/2*$^{-/-}$ Zymosan and Zymosan+IL-4c p=0.0029. Scale bar 50 µm. $^{*}p < 0.05$, $^{**}p < 0.01$, $^{***}p< 0.001$ and $^{****}p <0.0001$, ns not significant.

REFERENCES

1. Silverman, G.J., Gronwall, C., Vas, J. & Chen, Y. Natural autoantibodies to apoptotic cell membranes regulate fundamental innate immune functions and suppress inflammation. *Discov Med* **8**, 151-156 (2009).
2. Alugupalli, K.R. *et al.* B1b lymphocytes confer T cell-independent long-lasting immunity. *Immunity* **21**, 379-390 (2004).
3. Ochsenbein, A.F. *et al.* Control of early viral and bacterial distribution and disease by natural antibodies. *Science* **286**, 2156-2159 (1999).
4. Baumgarth, N. *et al.* B-1 and B-2 cell-derived immunoglobulin M antibodies are nonredundant components of the protective response to influenza virus infection. *J Exp Med* **192**, 271-280 (2000).
5. Haas, K.M., Poe, J.C., Steeber, D.A. & Tedder, T.F. B-1a and B-1b cells exhibit distinct developmental requirements and have unique functional roles in innate and adaptive immunity to S. pneumoniae. *Immunity* **23**, 7-18 (2005).
6. Boes, M., Prodeus, A.P., Schmidt, T., Carroll, M.C. & Chen, J. A critical role of natural immunoglobulin M in immediate defense against systemic bacterial infection. *J Exp Med* **188**, 2381-2386 (1998).
7. Martin, F., Oliver, A.M. & Kearney, J.F. Marginal zone and B1 B cells unite in the early response against T-independent blood-borne particulate antigens. *Immunity* **14**, 617-629 (2001).
8. Platell, C., Cooper, D., Papadimitriou, J.M. & Hall, J.C. The omentum. *World J Gastroenterol* **6**, 169-176 (2000).
9. Ansel, K.M., Harris, R.B. & Cyster, J.G. CXCL13 is required for B1 cell homing, natural antibody production, and body cavity immunity. *Immunity* **16**, 67-76 (2002).
10. Carlow, D.A., Gold, M.R. & Ziltener, H.J. Lymphocytes in the peritoneum home to the omentum and are activated by resident dendritic cells. *J Immunol* **183**, 1155-1165 (2009).
11. Ha, S.A. *et al.* Regulation of B1 cell migration by signals through Toll-like receptors. *J Exp Med* **203**, 2541-2550 (2006).
12. Rangel-Moreno, J. *et al.* Omental milky spots develop in the absence of lymphoid tissue-inducer cells and support B and T cell responses to peritoneal antigens. *Immunity* **30**, 731-743 (2009).
13. Elewa, Y.H., Ichii, O., Otsuka, S., Hashimoto, Y. & Kon, Y. Characterization of mouse mediastinal fat-associated lymphoid clusters. *Cell Tissue Res* (2014).

14. Moro, K. *et al.* Innate production of T(H)2 cytokines by adipose tissue-associated c-Kit(+)Sca-1(+) lymphoid cells. *Nature* **463**, 540-544 (2010).
15. Price, A.E. *et al.* Systemically dispersed innate IL-13-expressing cells in type 2 immunity. *Proc Natl Acad Sci U S A* **107**, 11489-11494 (2010).
16. Neill, D.R. *et al.* Nuocytes represent a new innate effector leukocyte that mediates type-2 immunity. *Nature* **464**, 1367-1370 (2010).
17. Spits, H. *et al.* Innate lymphoid cells--a proposal for uniform nomenclature. *Nat Rev Immunol* **13**, 145-149 (2013).
18. Randall, T.D., Carragher, D.M. & Rangel-Moreno, J. Development of secondary lymphoid organs. *Annu Rev Immunol* **26**, 627-650 (2008).
19. Roozendaal, R. & Mebius, R.E. Stromal cell-immune cell interactions. *Annu Rev Immunol* **29**, 23-43 (2011).
20. Ruddle, N.H. & Akirav, E.M. Secondary lymphoid organs: responding to genetic and environmental cues in ontogeny and the immune response. *J Immunol* **183**, 2205-2212 (2009).
21. Ngo, V.N. *et al.* Lymphotoxin alpha/beta and tumor necrosis factor are required for stromal cell expression of homing chemokines in B and T cell areas of the spleen. *J Exp Med* **189**, 403-412 (1999).
22. Krautler, N.J. *et al.* Follicular dendritic cells emerge from ubiquitous perivascular precursors. *Cell* **150**, 194-206 (2012).
23. Matsumoto, M. *et al.* Distinct roles of lymphotoxin alpha and the type I tumor necrosis factor (TNF) receptor in the establishment of follicular dendritic cells from non-bone marrow-derived cells. *J Exp Med* **186**, 1997-2004 (1997).
24. Ansel, K.M. *et al.* A chemokine-driven positive feedback loop organizes lymphoid follicles. *Nature* **406**, 309-314 (2000).
25. Fu, Y.X., Huang, G., Wang, Y. & Chaplin, D.D. B lymphocytes induce the formation of follicular dendritic cell clusters in a lymphotoxin alpha-dependent fashion. *J Exp Med* **187**, 1009-1018 (1998).
26. Yang, Y. *et al.* Antigen-specific memory in B-1a and its relationship to natural immunity. *Proc Natl Acad Sci U S A* **109**, 5388-5393 (2012).
27. Yang, Y. *et al.* Antigen-specific antibody responses in B-1a and their relationship to natural immunity. *Proc Natl Acad Sci U S A* **109**, 5382-5387 (2012).
28. Brennan, P.J., Brigl, M. & Brenner, M.B. Invariant natural killer T cells: an innate activation scheme linked to diverse effector functions. *Nat Rev Immunol* **13**, 101-117 (2013).

29. Marshall, J.L. *et al.* The capsular polysaccharide Vi from Salmonella typhi is a B1b antigen. *J Immunol* **189**, 5527-5532 (2012).
30. Gil-Cruz, C. *et al.* The porin OmpD from nontyphoidal Salmonella is a key target for a protective B1b cell antibody response. *Proc Natl Acad Sci U S A* **106**, 9803-9808 (2009).
31. Foote, J.B. & Kearney, J.F. Generation of B cell memory to the bacterial polysaccharide alpha-1,3 dextran. *J Immunol* **183**, 6359-6368 (2009).
32. Cascalho, M., Ma, A., Lee, S., Masat, L. & Wabl, M. A quasi-monoclonal mouse. *Science* **272**, 1649-1652 (1996).
33. Marshall, J.L. *et al.* Early B blasts acquire a capacity for Ig class switch recombination that is lost as they become plasmablasts. *Eur J Immunol* **41**, 3506-3512 (2011).
34. Casola, S. *et al.* Tracking germinal center B cells expressing germ-line immunoglobulin gamma1 transcripts by conditional gene targeting. *Proc Natl Acad Sci U S A* **103**, 7396-7401 (2006).
35. Muzumdar, M.D., Tasic, B., Miyamichi, K., Li, L. & Luo, L. A global double-fluorescent Cre reporter mouse. *Genesis* **45**, 593-605 (2007).
36. De Togni, P. *et al.* Abnormal development of peripheral lymphoid organs in mice deficient in lymphotoxin. *Science* **264**, 703-707 (1994).
37. Futterer, A., Mink, K., Luz, A., Kosco-Vilbois, M.H. & Pfeffer, K. The lymphotoxin beta receptor controls organogenesis and affinity maturation in peripheral lymphoid tissues. *Immunity* **9**, 59-70 (1998).
38. Sun, Z. *et al.* Requirement for RORgamma in thymocyte survival and lymphoid organ development. *Science* **288**, 2369-2373 (2000).
39. Koni, P.A. & Flavell, R.A. A role for tumor necrosis factor receptor type 1 in gut-associated lymphoid tissue development: genetic evidence of synergism with lymphotoxin beta. *J Exp Med* **187**, 1977-1983 (1998).
40. Kontoyiannis, D., Pasparakis, M., Pizarro, T.T., Cominelli, F. & Kollias, G. Impaired on/off regulation of TNF biosynthesis in mice lacking TNF AU-rich elements: implications for joint and gut-associated immunopathologies. *Immunity* **10**, 387-398 (1999).
41. Pabst, O. *et al.* Adaptation of solitary intestinal lymphoid tissue in response to microbiota and chemokine receptor CCR7 signaling. *J Immunol* **177**, 6824-6832 (2006).

42. Bouskra, D. *et al.* Lymphoid tissue genesis induced by commensals through NOD1 regulates intestinal homeostasis. *Nature* **456**, 507-510 (2008).
43. Hamada, H. *et al.* Identification of multiple isolated lymphoid follicles on the antimesenteric wall of the mouse small intestine. *J Immunol* **168**, 57-64 (2002).
44. Kamada, N., Seo, S.U., Chen, G.Y. & Nunez, G. Role of the gut microbiota in immunity and inflammatory disease. *Nat Rev Immunol* **13**, 321-335 (2013).
45. Grivennikov, S.I. *et al.* Distinct and nonredundant in vivo functions of TNF produced by t cells and macrophages/neutrophils: protective and deleterious effects. *Immunity* **22**, 93-104 (2005).
46. Ji, Y. *et al.* Short Term High Fat Diet Challenge Promotes Alternative Macrophage Polarization in Adipose Tissue via Natural Killer T Cells and Interleukin-4. *J Biol Chem* **287**, 24378-24386 (2012).
47. Ji, Y. *et al.* Activation of natural killer T cells promotes M2 Macrophage polarization in adipose tissue and improves systemic glucose tolerance via interleukin-4 (IL-4)/STAT6 protein signaling axis in obesity. *J Biol Chem* **287**, 13561-13571 (2012).
48. Lynch, L. *et al.* Adipose tissue invariant NKT cells protect against diet-induced obesity and metabolic disorder through regulatory cytokine production. *Immunity* **37**, 574-587 (2012).
49. Schipper, H.S. *et al.* Natural killer T cells in adipose tissue prevent insulin resistance. *J Clin Invest* (2012).
50. Wu, L. *et al.* Activation of invariant natural killer T cells by lipid excess promotes tissue inflammation, insulin resistance, and hepatic steatosis in obese mice. *Proc Natl Acad Sci U S A* **109**, E1143-1152 (2012).
51. Fukuyama, S. *et al.* Initiation of NALT organogenesis is independent of the IL-7R, LTbetaR, and NIK signaling pathways but requires the Id2 gene and CD3(-)CD4(+)CD45(+) cells. *Immunity* **17**, 31-40 (2002).
52. Oliphant, C.J. *et al.* MHCII-Mediated Dialog between Group 2 Innate Lymphoid Cells and CD4(+) T Cells Potentiates Type 2 Immunity and Promotes Parasitic Helminth Expulsion. *Immunity* **41**, 283-295 (2014).
53. Wong, S.H. *et al.* Transcription factor RORalpha is critical for nuocyte development. *Nat Immunol* **13**, 229-236 (2012).
54. Kwon, H. *et al.* Adipocyte-specific IKKbeta signaling suppresses adipose tissue inflammation through an IL-13-dependent paracrine feedback pathway. *Cell Rep* **9**, 1574-1583 (2014).

55. Erickson, L.D., Foy, T.M. & Waldschmidt, T.J. Murine B1 B cells require IL-5 for optimal T cell-dependent activation. *J Immunol* **166**, 1531-1539 (2001).
56. Benezech, C. *et al.* Lymphotoxin-beta receptor signaling through NF-kappaB2-RelB pathway reprograms adipocyte precursors as lymph node stromal cells. *Immunity.* **37**, 721-734. (2012).
57. Gil-Ortega, M. *et al.* Native adipose stromal cells egress from adipose tissue in vivo: evidence during lymph node activation. *Stem Cells* **31**, 1309-1320 (2013).
58. Carvalheira, J.B., Qiu, Y. & Chawla, A. Blood spotlight on leukocytes and obesity. *Blood* (2013).
59. Nikolajczyk, B.S., Jagannathan-Bogdan, M. & Denis, G.V. The outliers become a stampede as immunometabolism reaches a tipping point. *Immunol Rev* **249**, 253-275 (2012).
60. Odegaard, J.I. & Chawla, A. The immune system as a sensor of the metabolic state. *Immunity* **38**, 644-654 (2013).
61. Jenkins, S.J. *et al.* Local macrophage proliferation, rather than recruitment from the blood, is a signature of TH2 inflammation. *Science* **332**, 1284-1288 (2011).

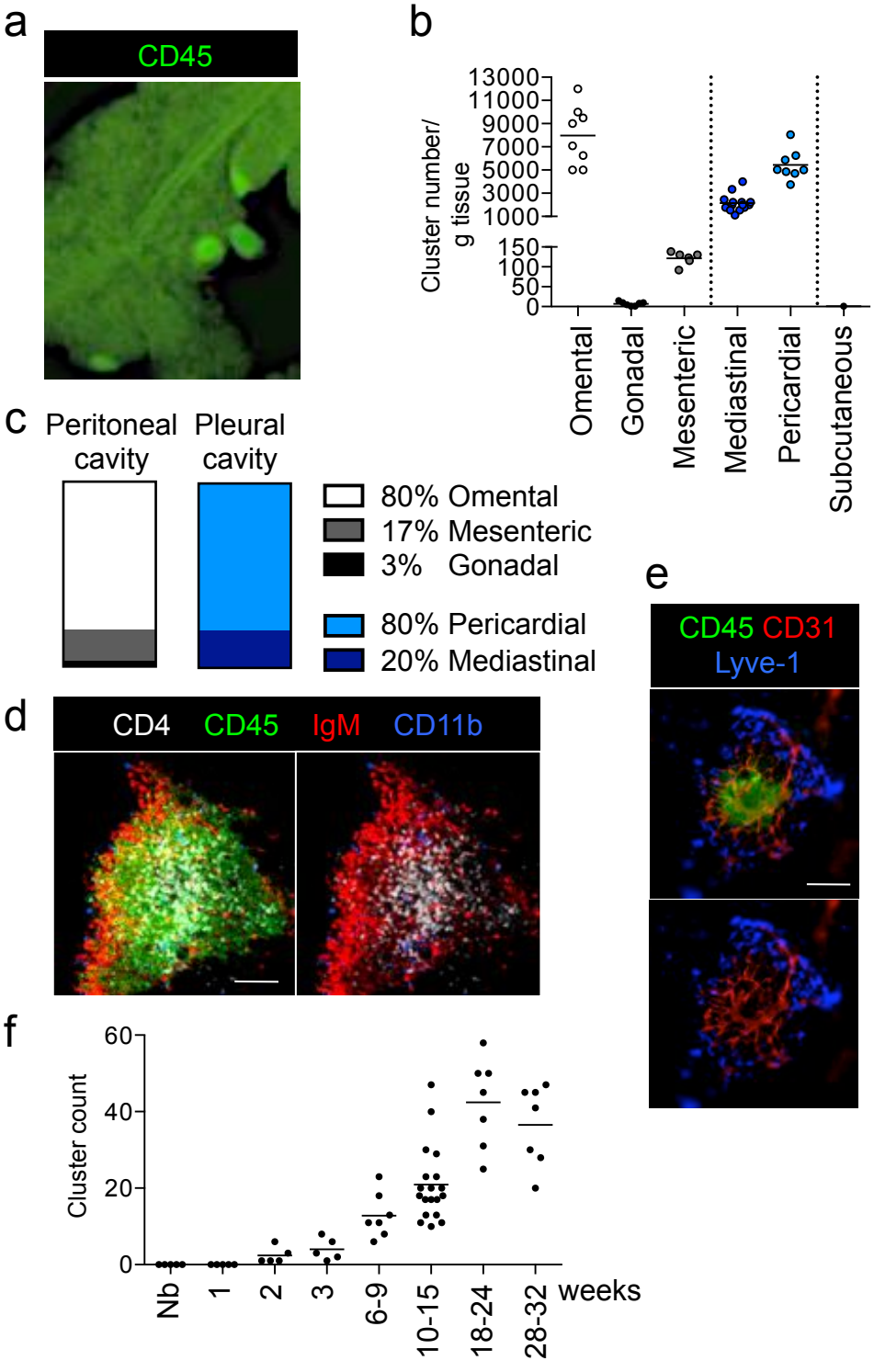
a
CD45
b
Cluster number/ g tissue
13000
11000
9000
7000
5000
3000
1000
150
100
50
0
Omental
Gonadal
Mesenteric
Mediastinal
Pericardial
Subcutaneous
c
Peritoneal cavity
Pleural cavity
80% Omental
17% Mesenteric
3% Gonadal
80% Pericardial
20% Mediastinal
d
CD4 CD45 IgM CD11b
e
CD45 CD31
Lyve-1
f
Cluster count
60
40
20
0
Nb
1
2
3
6-9
10-15
18-24
28-32
weeks

Figure 1

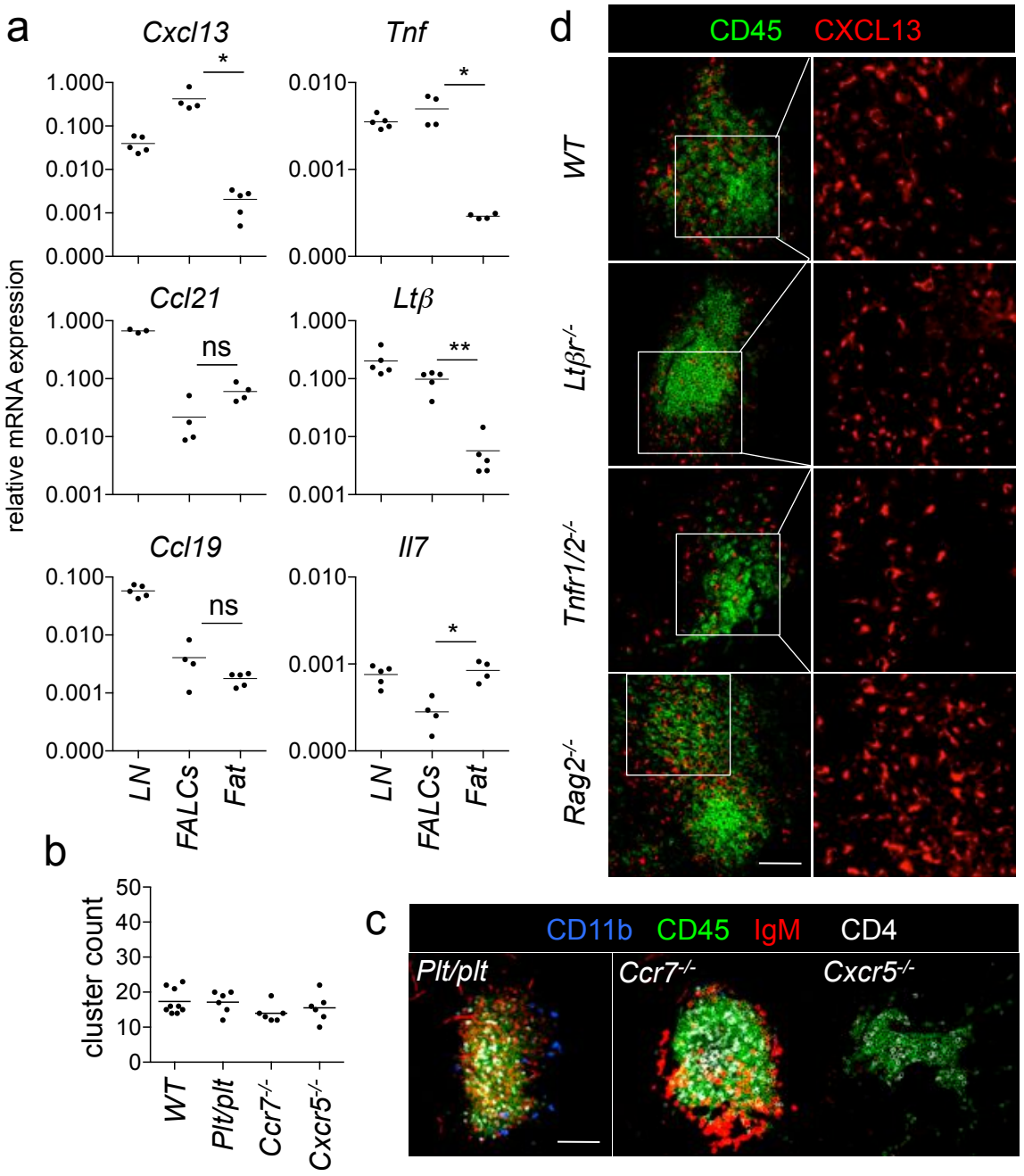
a
Cxcl13
Tnf
Ccl21
Ltβ
Ccl19
Il7
relative mRNA expression
1.000
0.100
0.010
0.001
0.000
0.010
0.001
0.000
*
ns
**
LN
FALCs
Fat
b
cluster count
50
40
30
20
10
0
WT
Plt/plt
Ccr7-/-
Cxcr5-/-
c
CD11b CD45 IgM CD4
Plt/plt
Ccr7-/-
Cxcr5-/-
d
CD45 CXCL13
WT
Ltβr-/-
Tnfr1/2-/-
Rag2-/-

Figure 2

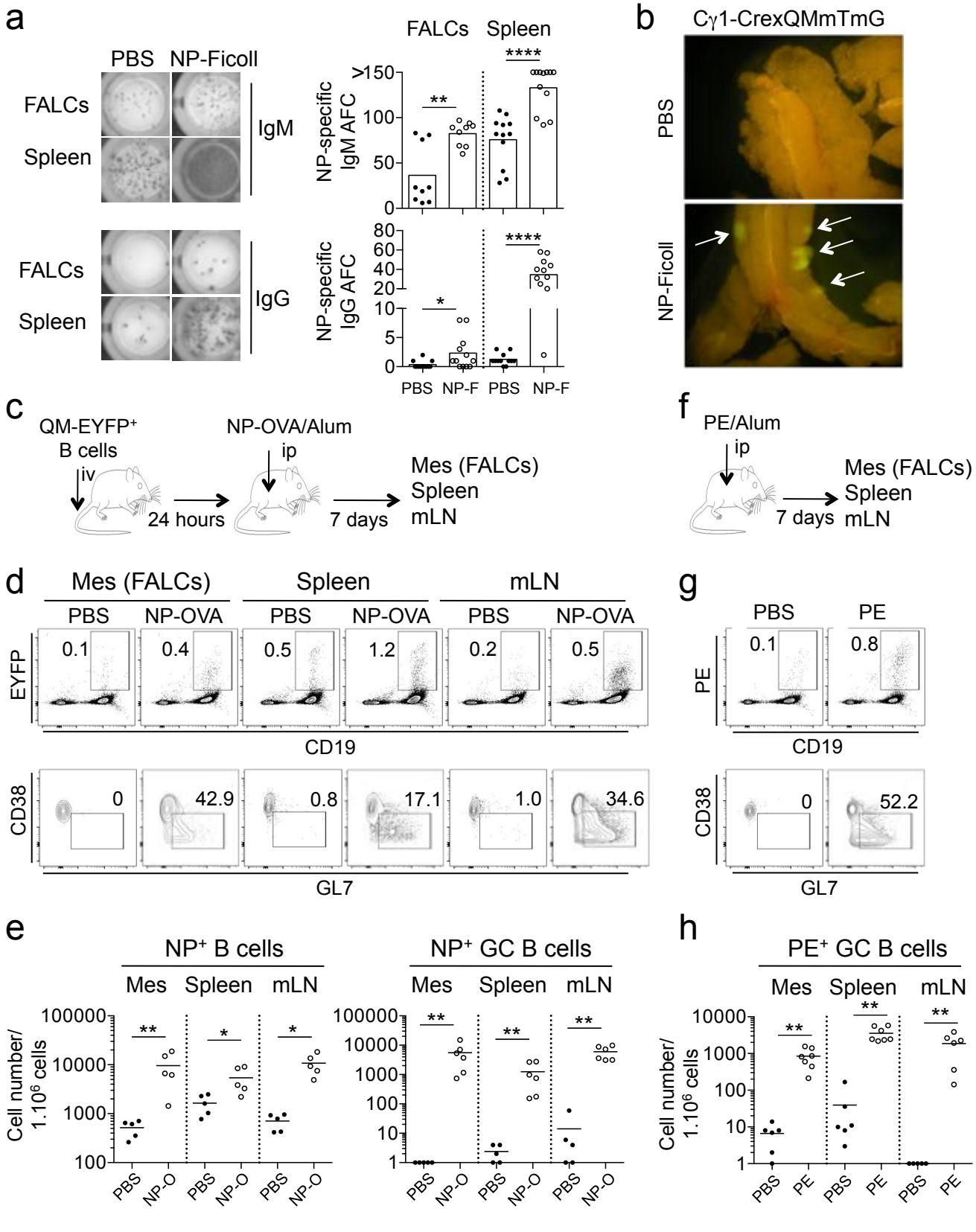
a
PBS
NP-Ficoll
FALCs
Spleen
IgM
IgG
FALCs
Spleen
NP-specific IgM AFC
NP-specific IgG AFC
PBS NP-F PBS NP-F
b
Cγ1-CrexQMmTmG
PBS
NP-Ficoll
c
QM-EYFP+ B cells
iv
24 hours
NP-OVA/Alum
ip
7 days
Mes (FALCs)
Spleen
mLN
f
PE/Alum
ip
7 days
Mes (FALCs)
Spleen
mLN
d
Mes (FALCs)
Spleen
mLN
PBS
NP-OVA
EYFP
CD19
CD38
GL7
0.1
0.4
0.5
1.2
0.2
0.5
0
42.9
0.8
17.1
1.0
34.6
g
PBS
PE
PE
CD19
CD38
GL7
0.1
0.8
0
52.2
e
NP+ B cells
NP+ GC B cells
Mes Spleen mLN
Cell number/ 1.10^6 cells
PBS NP-O
h
PE+ GC B cells
Mes Spleen mLN
Cell number/ 1.10^6 cells
PBS PE

Figure 3

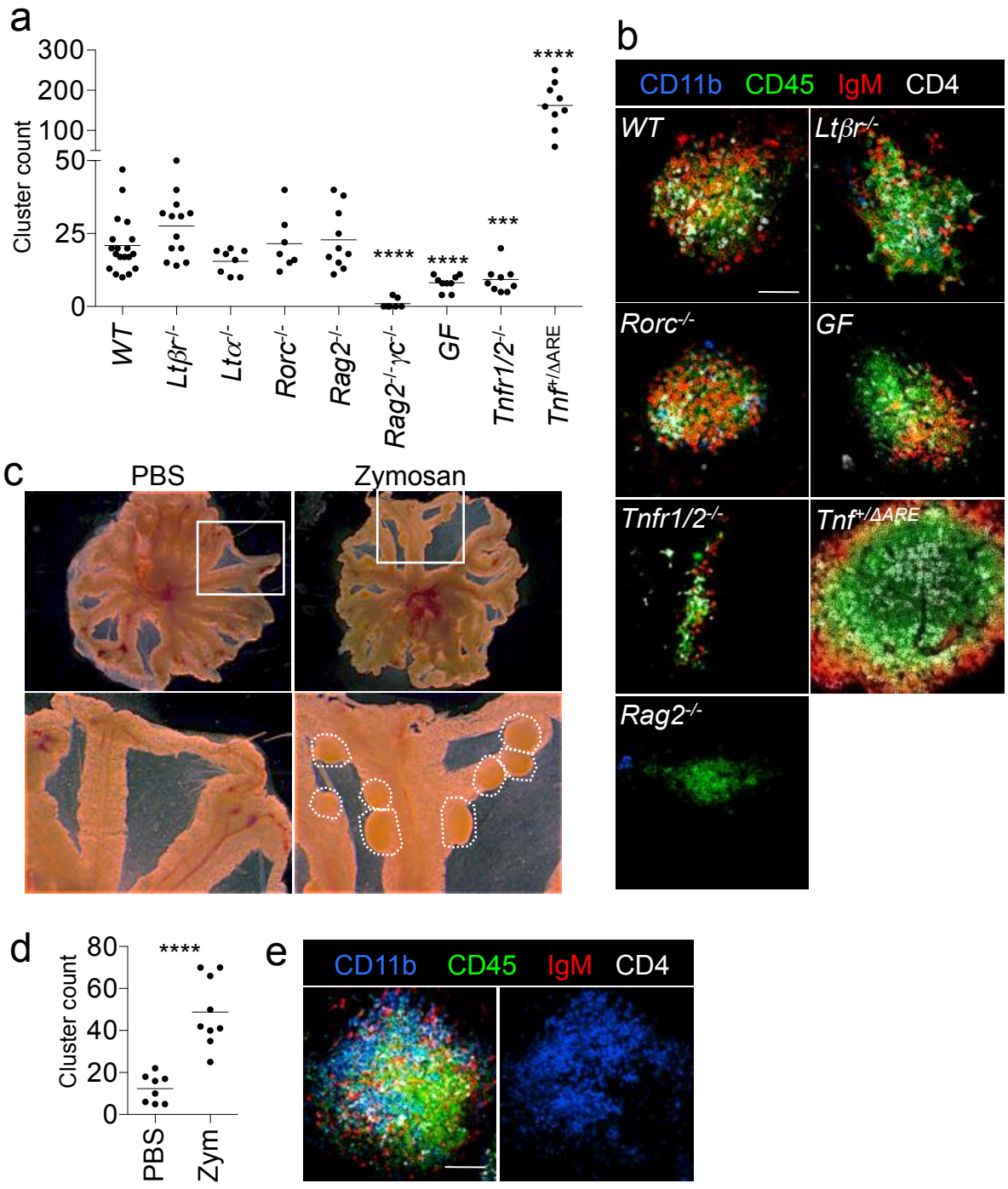
a
Cluster count
300
200
100
50
25
0
****
****
****
***
WT
Ltβr-/-
Ltα-/-
Rorc-/-
Rag2-/-
Rag2-/-γc-/-
GF
Tnfr1/2-/-
Tnf+/ΔARE
b
CD11b CD45 IgM CD4
WT
Ltβr-/-
Rorc-/-
GF
Tnfr1/2-/-
Tnf+/ΔARE
Rag2-/-
c
PBS
Zymosan
d
Cluster count
80
60
40
20
0
****
PBS
Zym
e
CD11b CD45 IgM CD4

Figure 4

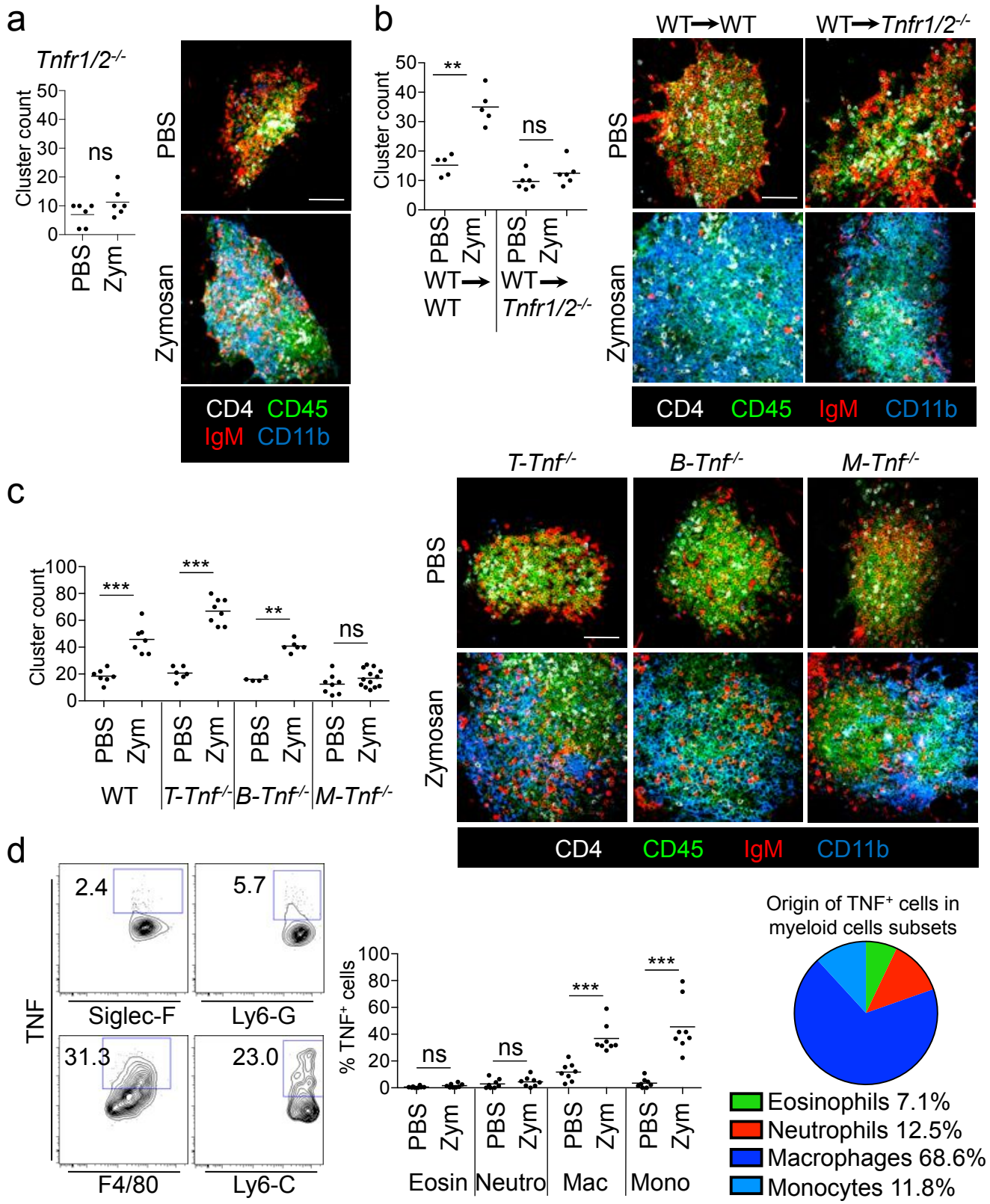
a
Tnfr1/2-/-
Cluster count
ns
PBS
Zym
PBS
Zymosan
CD4 CD45
IgM CD11b
b
Cluster count
**
ns
PBS
Zym
WT→WT
WT→Tnfr1/2-/-
PBS
Zymosan
CD4 CD45 IgM CD11b
c
T-Tnf-/-
B-Tnf-/-
M-Tnf-/-
Cluster count
***
**
ns
WT
T-Tnf-/-
B-Tnf-/-
M-Tnf-/-
d
2.4
5.7
31.3
23.0
TNF
Siglec-F
Ly6-G
F4/80
Ly6-C
% TNF+ cells
Eosin
Neutro
Mac
Mono
Origin of TNF+ cells in myeloid cells subsets
Eosinophils 7.1%
Neutrophils 12.5%
Macrophages 68.6%
Monocytes 11.8%

Figure 5

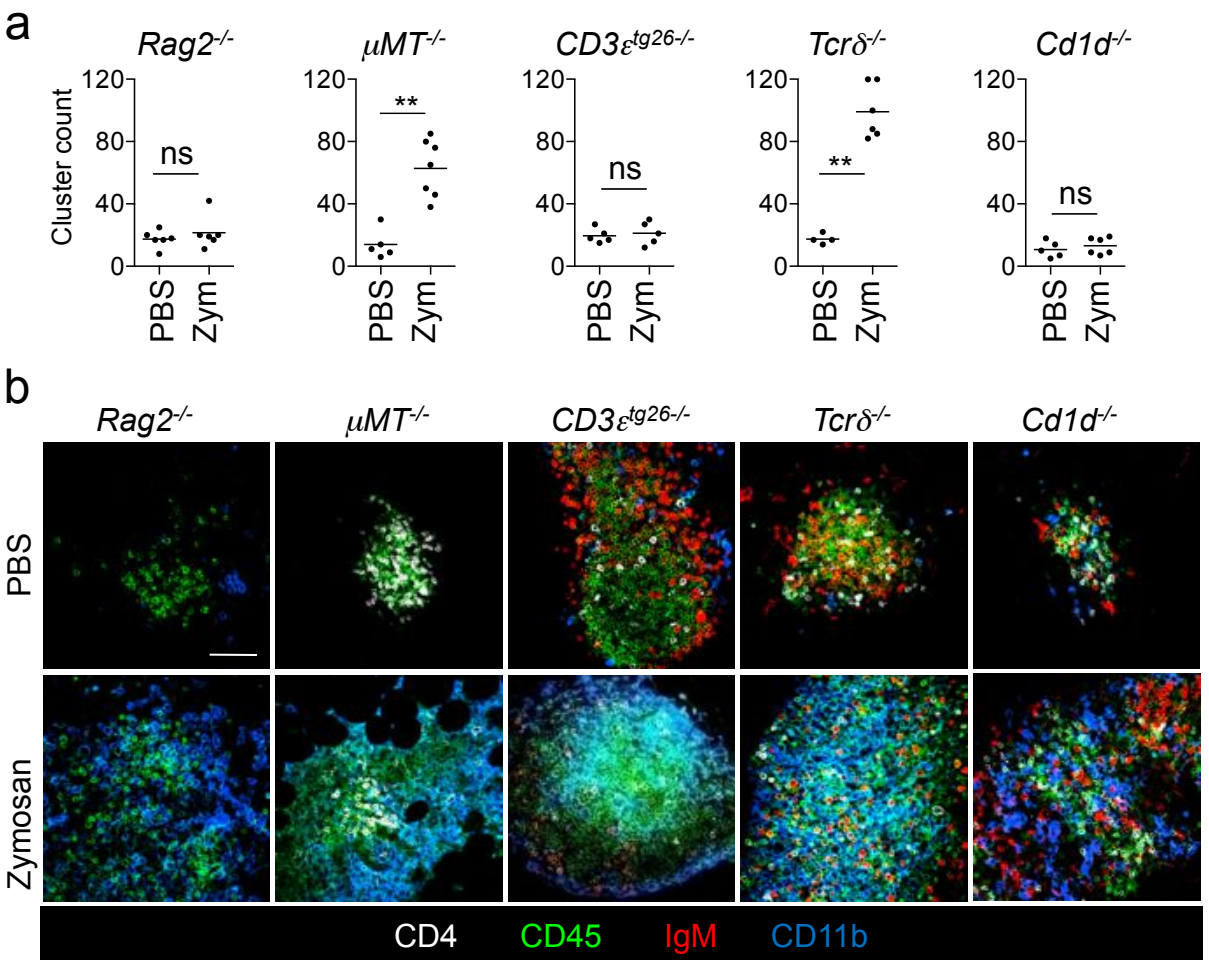
a
Rag2-/-
μMT-/-
CD3εtg26-/-
Tcrδ-/-
Cd1d-/-
Cluster count
120
80
40
0
ns
**
PBS
Zym
b
PBS
Zymosan
CD4
CD45
IgM
CD11b

Figure 6

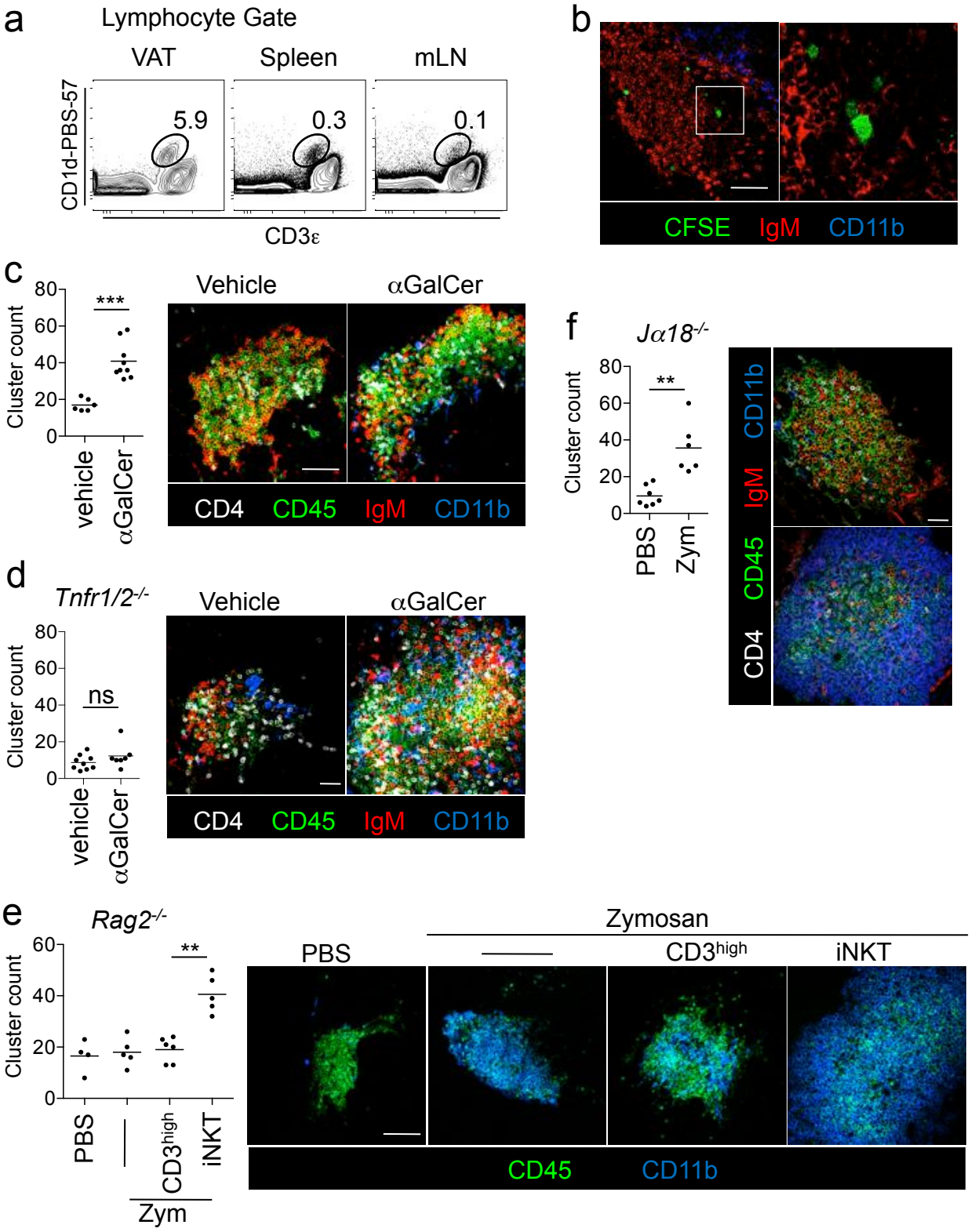
a
Lymphocyte Gate
VAT
Spleen
mLN
CD1d-PBS-57
5.9
0.3
0.1
CD3ε
b
CFSE
IgM
CD11b
c
Cluster count
***
vehicle
αGalCer
Vehicle
αGalCer
CD4
CD45
IgM
CD11b
d
Tnfr1/2-/-
ns
e
Rag2-/-
**
PBS
CD3high
iNKT
Zym
Zymosan
f
Jα18-/-
PBS
Zym

Figure 7

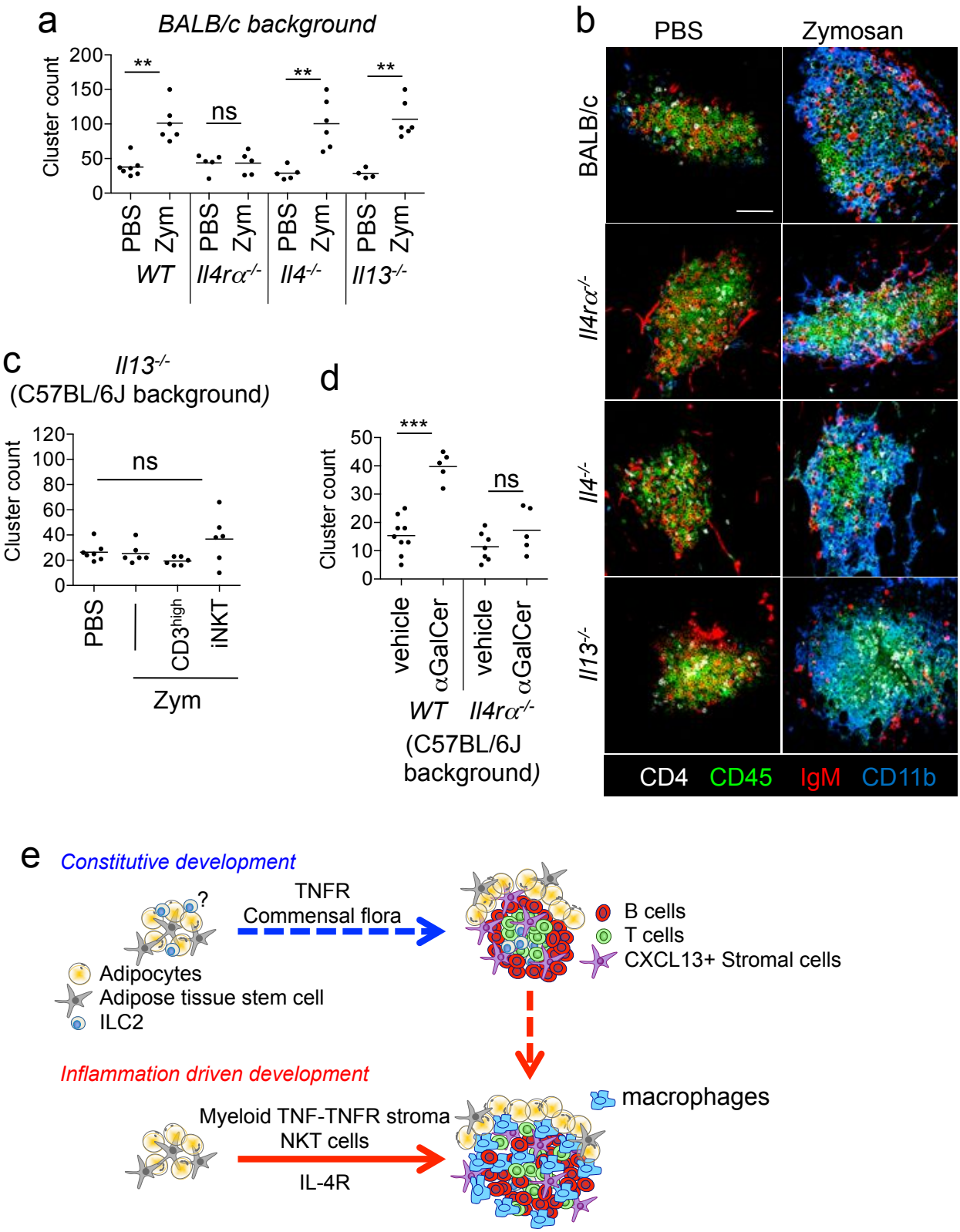
a
BALB/c background
Cluster count
200
150
100
50
0
**
ns
**
**
PBS
Zym
PBS
Zym
PBS
Zym
PBS
Zym
WT
Il4rα-/-
Il4-/-
Il13-/-
b
PBS
Zymosan
BALB/c
Il4rα-/-
Il4-/-
Il13-/-
CD4 CD45 IgM CD11b
c
Il13-/-
(C57BL/6J background)
Cluster count
120
100
80
60
40
20
0
ns
PBS
CD3high
iNKT
Zym
d
Cluster count
50
40
30
20
10
0
***
ns
vehicle
αGalCer
vehicle
αGalCer
WT
Il4rα-/-
(C57BL/6J background)
e
Constitutive development
?
TNFR
Commensal flora
B cells
T cells
CXCL13+ Stromal cells
Adipocytes
Adipose tissue stem cell
ILC2
Inflammation driven development
macrophages
Myeloid TNF-TNFR stroma
NKT cells
IL-4R

Figure 8

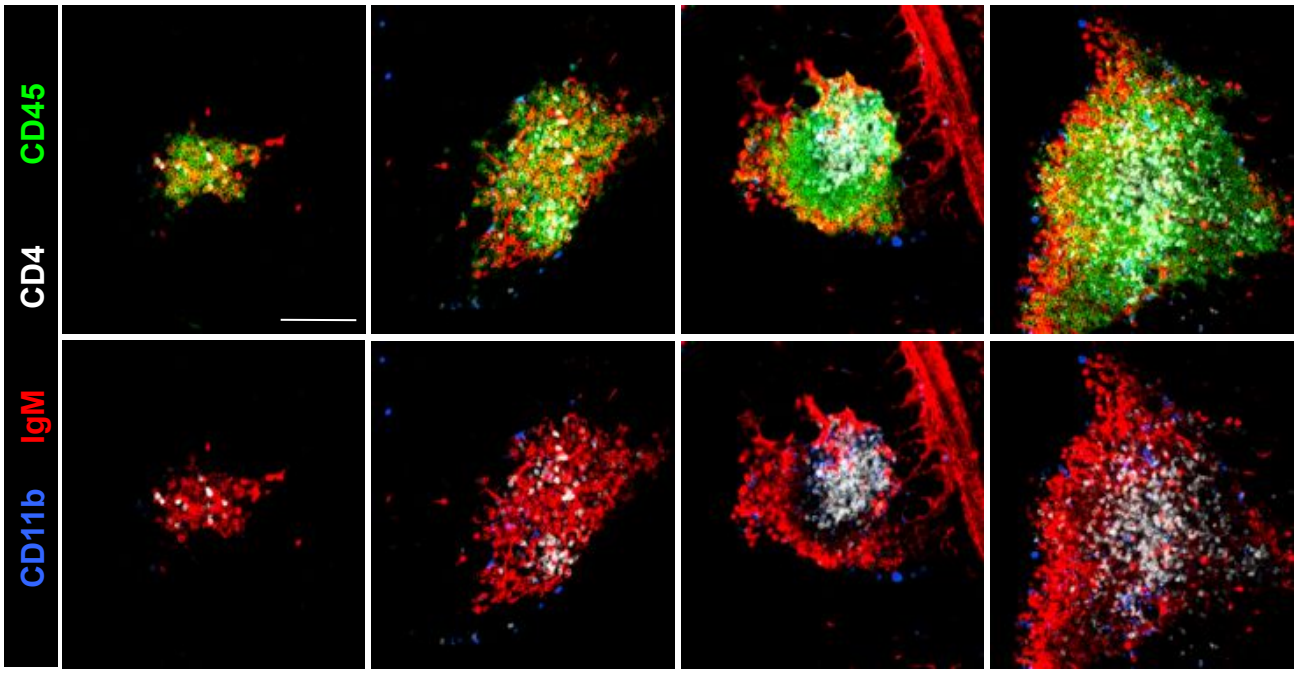

Supplementary Figure 1

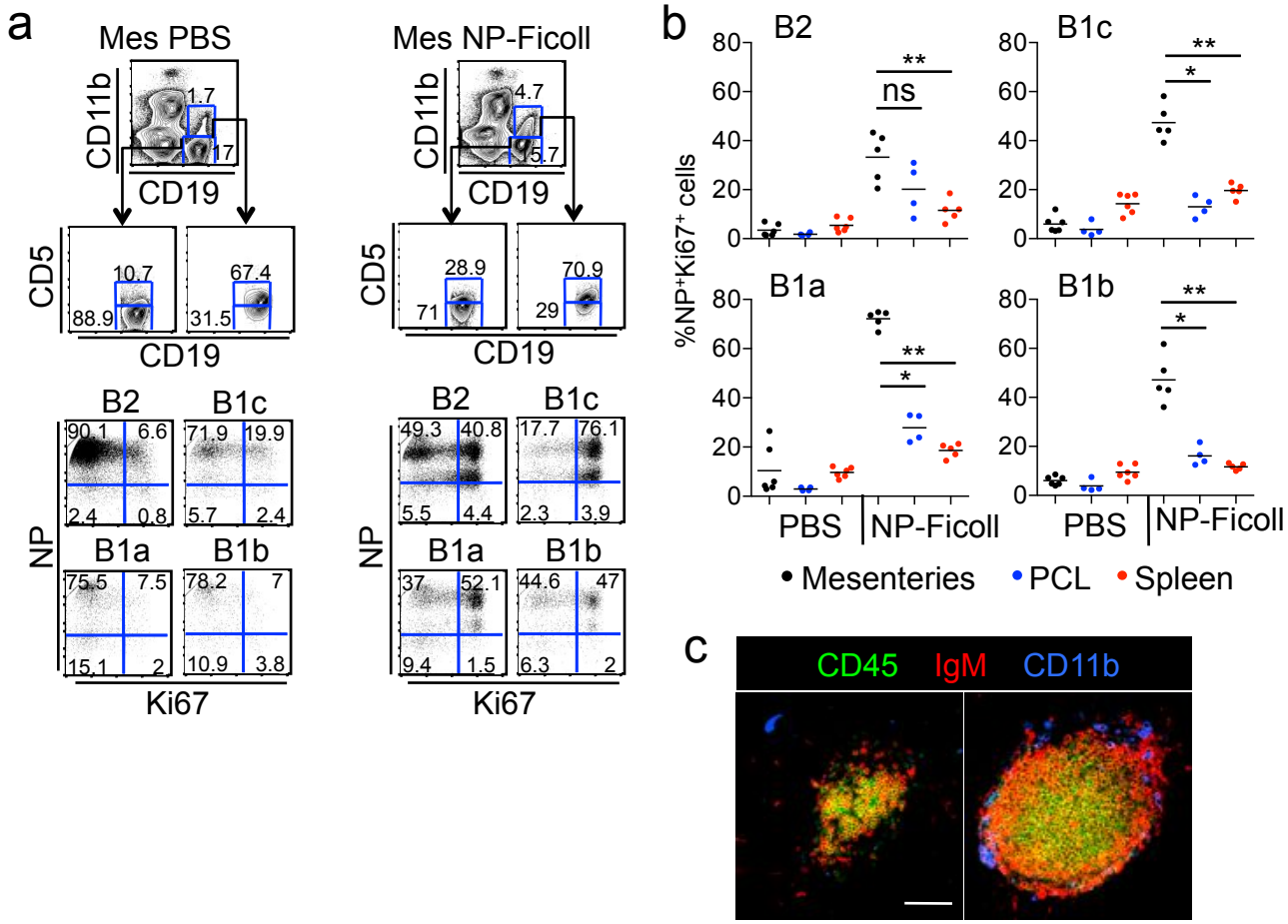

Supplementary Figure 2

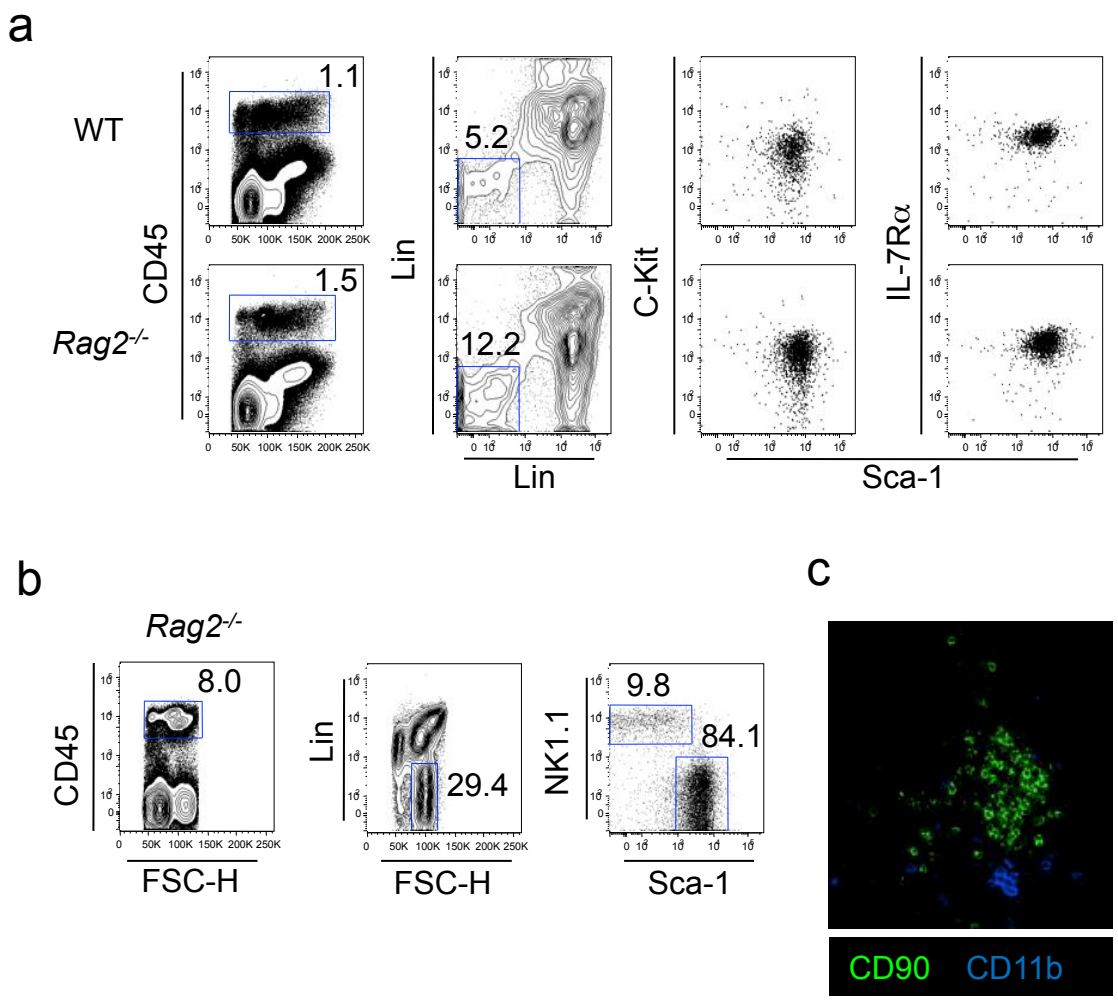

Supplementary Figure 3

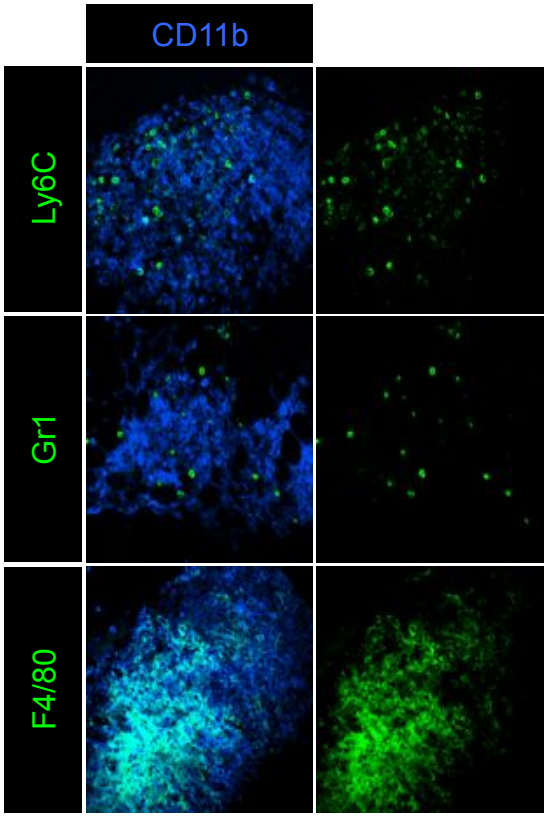

Supplementary Figure 4

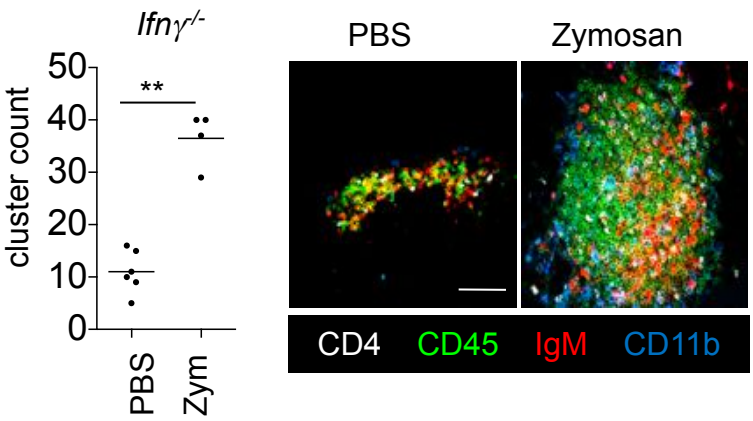

Supplementary Figure 5

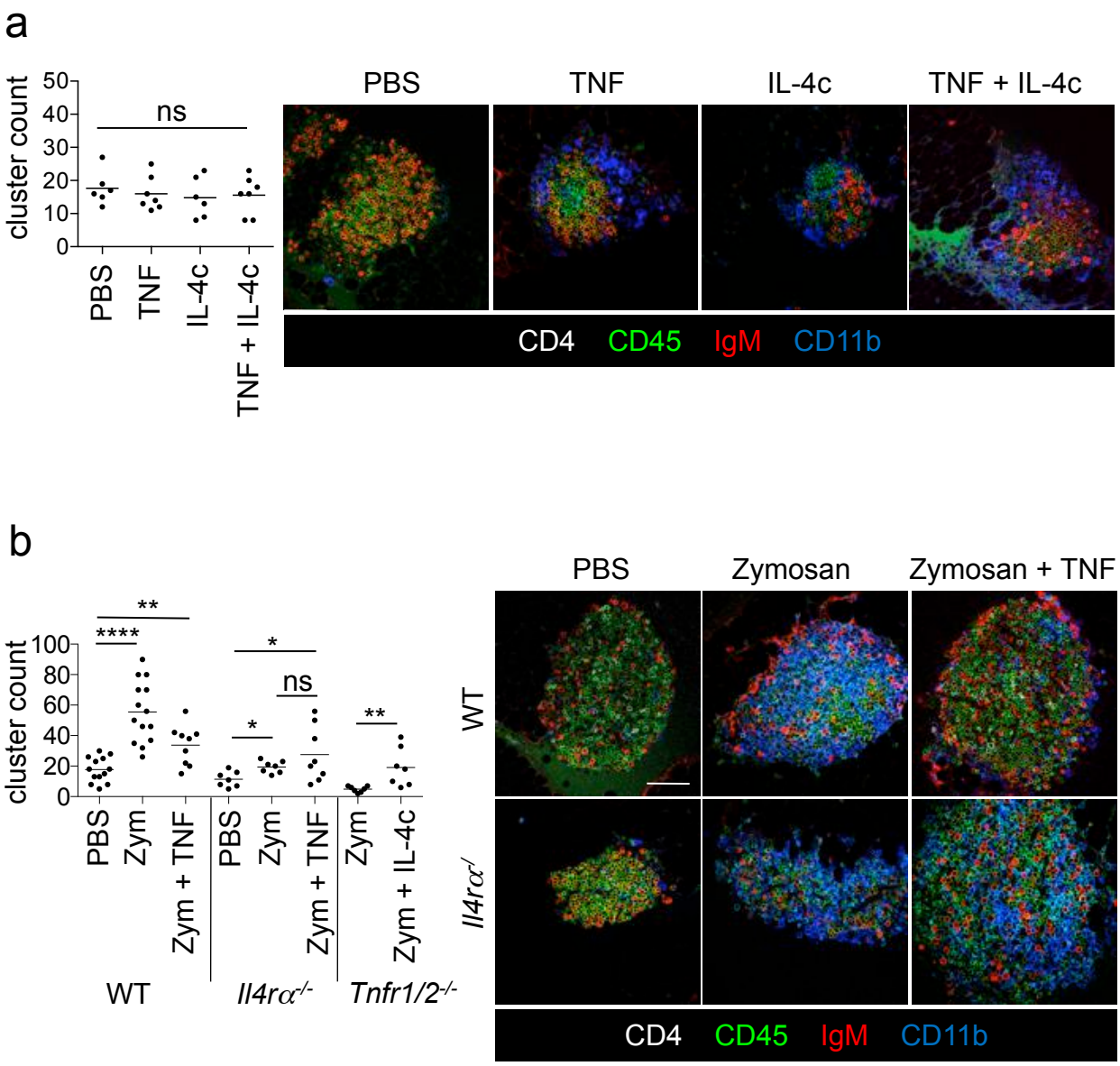

Supplementary Figure 6